

A novel miR-99b-5p-Zbp1 pathway in microglia contributes to the pathogenesis of schizophrenia

2

3 Lalit Kaurani^{*#1}, Md Rezaul Islam^{*1}, Urs Heilbronner^{*2}, Dennis M. Krüger¹, Jiayin Zhou¹, Aditi Methi¹,
4 Judith Strauss³, Ranjit Pradhan¹, Susanne Burkhardt¹, Tonatiuh Pena¹, Lena Erlebach⁴, Anika Bühler⁴,
5 Monika Budde², Fanny Senner², Mojtaba Oraki Kohshour², Eva C. Schulte^{2,5,, 6,7}, Max Schmauß⁸, Eva Z.
6 Reininghaus⁹, Georg Juckel¹⁰, Deborah Kronenberg-Versteeg⁴, Ivana Delalle¹¹, Francesca Odoardi³,
7 Alexander Flügel³, Thomas G. Schulze^{#2}, Peter Falkai^{#5}, Farahnaz Sananbenesi^{#12}, Andre Fischer^{#1,13,14}

8 * These authors contributed equally to this work

9

Co-corresponding authors lalit.kaurani@dzne.de; thomas.schulze@med.uni-muenchen.de
10 peter.falkai@med.uni-muenchen.de; fsananb@gwdg.de;
11 a.fischer@mail.gwdg.de

12 ¹Department for Epigenetics and Systems Medicine in Neurodegenerative Diseases, German Center for
13 Neurodegenerative Diseases (DZNE) Goettingen, 37077 Goettingen, Germany

14 ²Institute of Psychiatric Phenomics and Genomics (IPPG), University Hospital, LMU Munich, Germany

15 ³Institute for Neuroimmunology and Multiple Sclerosis Research, University Medical Center Göttingen,
16 Göttingen, Germany

17 ⁴Department of Cellular Neurology, Hertie Institute for Clinical Brain Research, University of Tübingen,
18 Germany; Germany and German Center for Neurodegenerative Diseases (DZNE) Tübingen, Germany

19 ⁵Department of Psychiatry and Psychotherapy, University Hospital, LMU Munich, Germany

20 ⁶Department of Psychiatry and Psychotherapy, University Hospital Bonn, Medical Faculty, University of Bonn,
21 Bonn, Germany.

22 ⁷Institute of Human Genetics, University Hospital Bonn, Medical Faculty, University of Bonn, Bonn, Germany.

23 ⁸Clinic for Psychiatry, Psychotherapy and Psychosomatics, Augsburg University, Medical Faculty,
24 Bezirkskrankenhaus Augsburg, Augsburg, 86156, Germany

25 ⁹Department of Psychiatry and Psychotherapeutic Medicine, Research Unit for Bipolar Affective Disorder,
26 Medical University of Graz, Graz, 8036, Austria

27 ¹⁰Department of Psychiatry, Ruhr University Bochum, LWL University Hospital, Bochum, 44791, Germany

28 ¹¹Department of Pathology, Lifespan Academic Medical Center, Alpert Medical School of Brown University,
29 Providence, RI 02903, USA

30 ¹²Research Group for Genome Dynamics in Brain Diseases, 37077 Goettingen, Germany.

31 ¹³Department of Psychiatry and Psychotherapy, University Medical Center Goettingen, 37077 Goettingen,
32 Germany

33 ¹⁴Cluster of Excellence "Multiscale Bioimaging: from Molecular Machines to Networks of Excitable Cells"
34 (MBExC), University of Göttingen, Germany

35

36

37 Abstract

38 Schizophrenia is a psychiatric disorder that is still not readily treatable. Pharmaceutical advances in
39 the treatment of schizophrenia have mainly focused on the protein coding part of the human genome.
40 However, the vast majority of the human transcriptome consists of non-coding RNAs. MicroRNAs are
41 small non-coding RNAs that control the transcriptome at the systems level. In the present study we
42 analyzed the microRNAome in blood and postmortem brains of controls and schizophrenia patients
43 and found that miR-99b-5p was downregulated in both the prefrontal cortex and blood of patients.
44 At the mechanistic level we show that inhibition of miR-99b-5p leads to schizophrenia-like phenotypes
45 in mice and induced inflammatory processes in microglia linked to synaptic pruning. The miR-99b-5p-
46 mediated inflammatory response in microglia depended on *Z-DNA binding protein 1 (Zbp1)* which we
47 identified as a novel miR-99b-5p target. Antisense oligos (ASOs) against *Zbp1* ameliorated the
48 pathological phenotypes caused by miR-99b-5p inhibition. In conclusion, we report a novel miR-99b-
49 5p-*Zbp1* pathway in microglia that contributes to the pathogenesis of schizophrenia. Our data suggest
50 that strategies to increase the levels of miR-99b-5p or inhibit *Zbp1* could become a novel therapeutic
51 strategy.

53 Introduction

54
55 Schizophrenia (SZ) is a devastating psychiatric disorder, and the difficulties involved in treating and
56 managing it make it one of the ten most expensive disorders for health care systems worldwide ^{1 2}. SZ
57 is believed to evolve on the background of complex genome-environment interactions that alter the
58 cellular homeostasis as well as the structural plasticity of brain cells. Thus, genetic predisposition and
59 environmental risk factors seem to affect processes that eventually contribute to the manifestation
60 of clinical symptoms ^{3 4 5}. Despite the available pharmacological and non-pharmacological treatment
61 options, a significant number of patients do not benefit from these treatments in the long-term,
62 underscoring the need for novel and potentially stratified therapeutic approaches ⁶. So far, drug
63 development has focused on the human transcriptome that encodes proteins, but the success of this
64 approach is limited ⁷. However, most of the transcriptome consists of non-coding RNAs (ncRNAs)
65 which are recognized as key regulators of cellular functions ⁸. Therefore, RNA therapeutics represent
66 an emerging concept that may expand current therapeutic strategies focused on the protein-coding
67 part of our genome ^{9 10}. RNA therapies utilize, for example, antisense oligonucleotides (ASOs), siRNA,
68 microRNA (miR) mimics or corresponding anti-miRs to control the expression of genes and proteins
69 implicated in disease onset and progression ^{11 9}. Of particular interest are miRs, which are 19-22
70 nucleotide-long RNA molecules that regulate protein homeostasis via binding to target mRNAs,

leading either to their degradation or reduced translation¹². miRs have been intensively studied as biomarkers and therapeutic targets in cancer¹¹ and cardiac diseases¹³. There is also emerging evidence from genetic studies in humans as well as functional data from mouse models that miRs play a role in CNS diseases including SZ^{14 15 16 17}. In addition, several studies reported changes in miR expression in blood samples of SZ patients using either qPCR analysis of selected targets or genome-wide approaches. The current findings have been summarized in several review articles^{18 19 20}. Despite this progress, there are still only few reports on the function of candidate miRs²¹. Nevertheless, analysis of miRs in liquid biopsies is highly valuable because one miR can affect many target genes, and thus changes in miR expression can indicate the presence of multiple pathologies^{22 14 23}. Moreover, miRs also participate in inter-organ communication^{24 25}, suggesting that alterations of miR expression in liquid biopsies may inform about relevant pathological processes in other organs, including the brain. This is important since the analysis of the molecular processes underlying neuropsychiatric diseases in post-mortem human brain tissue is challenging because it might be affected e.g. by peri-mortem events or the timing of post-mortem tissue sampling. Furthermore, the onset of the disease often precedes tissue collection by decades. In contrast, liquid biopsies such as blood samples are easy to collect on the premise that molecular changes in blood mirror changes in the brain. In this context, the analysis of the microRNAome in liquid biopsies could be a suitable approach to identify candidate microRNAs that may play a role in the onset and progression of SZ.

89

In the present study we performed small RNA sequencing in blood samples of control participants (n = 331) and schizophrenia patients (n = 242) of the PsyCourse Study²⁶ (<http://www.psycourse.de/>). By cross-correlating our findings with data from post-mortem human brain tissue, we identified miR-99b-5p as a promising biomarker candidate that is decreased in blood and in the prefrontal cortex of SZ patients, and correlates with disease phenotypes. Furthermore, we found decreased levels of miR-99b-5p in the prefrontal cortex of mice to elicit SZ-like phenotypes and activate pathways linked to innate immunity. In line with these observations, inhibition of miR-99b-5p in microglia increased phagocytosis and reduced the number of synapses. Finally, we were able to demonstrate that this effect is controlled by the miR-99b-5p target gene *Zbp1*, an upstream regulator of innate immunity²⁷. Taken together, our data suggest that targeting miR-99b-5p or its target *Zbp1* could provide a novel approach towards the treatment of SZ patients.

101

102 **Results**

103 *miR-99b-5p expression is decreased in SZ patients*

To identify microRNAs that play a role in the pathogenesis of SZ, we conducted small RNA sequencing of blood samples obtained from 573 participants of the PsyCourse Study (<http://www.psycourse.de/>). We analyzed 331 healthy controls and 242 SZ patients (**Fig. 1a, Fig. S1, supplemental table 1**)²⁶. After data normalization and correction for confounding factors, we performed a weighted gene co-expression network analysis (WGCNA) and detected 8 co-expression modules that significantly differed between groups. Three were significantly decreased (**Fig. 1b**) while 5 were increased (**Fig. 1c**) in SZ patients (**supplemental table 2**). The turquoise, yellow, blue and red modules displayed the most significant differences among the groups ($P < 0.0001$). We then investigated whether the expression levels of any of these modules correlated with the clinical phenotypes defined by the positive and negative syndrome rating scale (PANSS) and Beck depression inventory (BDI-II), both of which are decreased in SZ patients, and/or the global assessment of functioning (GAF) score, which is increased in these patients (**Fig. S1**). Out of the 8 co-expression modules the turquoise, yellow, blue and red modules were significantly correlated to all disease phenotypes. The turquoise module exhibited a significant negative correlation to the PANSS and BDI-II score and a positive correlation with the GAF score (**Fig. 1d**), which is in line with the decreased expression of this module in SZ. The green, yellow, blue and red modules were positively correlated to the PANSS and BDI-II scores and exhibited a negative correlation with the GAF score, which is in agreement with their increased expression in SZ (**Fig. 1d**). The pink module was negatively correlated to the PANSS scores and positively correlated to the GAF, which is also in agreement with its decreased expression in SZ patients. However, the pink module was not correlated to the BDI-II score (**Fig. 1d**). The black and the brown modules were not significantly correlated any of the analyzed phenotypes. Taken together, these data suggest that especially the microRNAs present in turquoise, pink, green, blue, yellow and red modules warrant further analysis. When we subjected the confirmed targets of the microRNAs present within each of these modules to a GO-term analysis, we observed that most modules were linked to inflammatory processes, which is in agreement with a suggested role of neuro-inflammation in the pathogenesis of SZ²⁸ (**Fig. S2; Supplemental table 3**). While WGCNA is a suitable first approach to identify groups of candidate microRNAs, we also performed a differential expression analysis to directly compare the microRNAome in control vs SZ patients. We found 59 microRNA that were significantly increased in SZ patients while 34 microRNAs were decreased (**Fig 1e, Supplemental table 4**).

With the aim to further refine the list of candidate microRNAs that may play a role in the pathogenesis of SZ, we performed small RNA sequencing from the prefrontal cortex of SZ patients (n=13) and controls (n=17). We detected 36 microRNAs that were significantly decreased in SZ patients (FDR < 0,01, log2FC > 1) and 32 that were significantly upregulated (**Fig. 1f, supplemental table 5**). Next, we examined whether any of these microRNAs are also found among the differentially expressed

microRNAs that were altered in blood samples when compared via differential expression analysis, and within the co-expression modules decreased in SZ patients. Three miRs of the yellow cluster were significantly increased in the brain and in the blood when analyzed via differential expression analysis. In addition, one miR of the blue and one of the green clusters were also increased in brain and blood. These were miR-101-3p, miR-378a-3p, miR-21-5p, miR-192-5p and miR-103a-3p (**supplemental table 6**). MiR- 21-3p has been associated with SZ while the other 4 miRs have been studied in the context of other neuropsychiatric or neurodegenerative diseases (**supplemental table 6**). When analyzing the down-regulated miRs we found four microRNAs, namely miR-500a-3p, miR-501-3p, miR-221-5p and miR-99b-5p, that were detected in the turquoise module and were also decreased in the postmortem brain of SZ patients (**Fig. 1g**). Of these 4 microRNAs miR-501-3p has been recently linked to schizophrenia²¹ (**supplemental table 6**) while miR-99b-5p was the only candidate that was part of a significantly downregulated co-expression module and was significantly downregulated in the brain and blood of SZ patients when analyzed via differential expression analysis. In summary, our data reveal a number of interesting candidate miRs such as miR-501-3p and miR-21-5p that have been already linked to SZ in previous studies^{29 21}. Most of the other miRs have been detected in the context of other brain diseases including Alzheimer's disease (AD), Major depression (MD) or Amyotrophic lateral sclerosis (ALS) (**supplemental table 6**). Except for miR-500a-3p and miR-221-5p, the expression of all other candidate miRs have is significantly correlated to the PANSSs, GAF and BDI-II scores (**Fig. 1h, Fig. S3**). While all of these candidate miRs would warrant further functional analysis in the context of SZ, we decided to focus on miR-99b-5p since it has not been linked to any brain disease yet and comparatively little is known about this miR in general.

Decreasing miR-99b-5p leads to SZ-like phenotypes in mice and the upregulation of genes linked to inflammatory processes

The role of miR-99b-5p in the brain has not been intensively studied and thus no data are available in the context of neuropsychiatric diseases such as SZ, making it a novel candidate in need of further evaluation. Before performing mechanistic studies, we decided to employ mice in a model system to test the hypothesis that decreased expression of miR-99b-5p is causatively linked to the development of SZ-like phenotypes. Therefore, we generated lipid nanoparticles (LNPs) containing locked nucleic acid (LNA) representing miR-99b-5p inhibitors (anti-miR99b) and injected these into the prefrontal cortex (PFC) of mice. LNAs representing a scrambled sequence were used as controls (sc-control). MiR-99b-5p levels were significantly decreased in the PFC when measured 5 or 10 days after the injections (**Fig 2a**). To test schizophrenia-like behaviors in animals, we injected either anti-miR-99b or sc-control to the PFC of mice. Explorative behavior measured in the open field test was similar in all groups (**Fig**

2b). However, anti-miR-99b-treated mice spent less time in the center of the open field, which is indicative of increased anxiety (**Fig 2c**), a phenotype commonly observed in schizophrenia patients³⁰. We also analyzed anxiety behavior in the elevated plus maze test. Anti-miR-99b treated mice spent less time in the open arms, which indicates increased anxiety (**Fig 2d**). Another valid animal model to test schizophrenia-like behavior in rodents is the pre-pulse inhibition of the startle response (PPI) which is used to measure sensory-gating function³¹. PPI is impaired in SZ patients, can easily be assayed in mice and is impaired in mouse models for SZ^{32 33}. We observed that mice injected with anti-miR-99b displayed significantly impaired PPI responses when compared to the sc-control group (**Fig 2e**). The basic startle response was unaffected (**Fig. 2f**), suggesting that decreasing the levels of miR-99b-5p in the PFC of mice can lead to SZ-like phenotypes.

To gain first insights into the molecular processes controlled by miR-99b-5p in the brain, we injected another group of mice with anti-miR-99b and sc-control oligonucleotides and isolated PFC tissue 5 days later for RNA sequencing analysis. Differential expression analysis revealed 147 deregulated genes (adjusted *p*-value < 0.1, log2FC +/- 0.2), of which 113 genes were upregulated and 34 were downregulated (**Fig. 2g; supplemental table 7**). Gene ontology (GO) analysis revealed that upregulated genes were linked to processes such as innate immunity and interferon signaling (**Fig. 2h**). GO analysis of the downregulated genes did not yield any highly significant pathways but detected processes linked to voltage-gated potassium channels (**Fig 2h, supplemental table 8**). These data suggest that miR-99b-5p in the PFC may regulate mRNAs linked to immune-related processes. To further test this hypothesis, we compared the list of upregulated genes with gene expression data from neurons, astrocytes and microglia as well as genes present within 3 different immune function-related gene expression databases. We observed that the upregulated genes were highly enriched in microglia ($P = 4 \times 10^{-12}$), while no enrichment was observed in astrocytes or neurons. The downregulated genes were significantly enriched in neurons ($P = 1.38 \times 10^{-12}$). In line with this, the upregulated genes were significantly overrepresented in 3 databases for genes linked to immune function, namely the immune, immunome and IRIS databases (**Fig. 2i**). Together, these data suggest that the levels of miR-99b-5p in the PFC of mice may specifically increase the expression of immune-related genes in microglia. To further test this we administered anti-miR-99b or sc-control to the PFC of mice and subsequently isolated CD45^{low}/CD11b⁺ microglial cells via fluorescence-activated cell sorting (FACS). While microglia cell numbers did not differ between groups, miR-99b-5p expression was significantly decreased in microglia isolated from anti-miR-99b-treated mice (**Fig. S4**). The expression of selected pro-inflammatory genes *Il1 β* , *Tgfb1* and *Tnfa* that were upregulated in the RNA-seq dataset were also increased in microglia obtained from anti-miR-99b-treated mice, although *Tgfb1* failed to reach significance ($P = 0.08$) (**Fig 2j**).

These data suggest that miR-99b-5p controls microglia-mediated immunity in the PFC, which is in agreement with previous studies linking aberrant microglia function and neuroinflammation to the pathogenesis of SZ³⁴.

miR-99b-5p controls microglia-mediated immune function and affects dendritic spine number

To further explore the role of miR-99b-5p in microglia, we cultured primary microglia from the cortex of mice and treated these cells with anti-miR-99b or sc-control LNAs followed by RNA sequencing (**Fig 3a**). Differential expression analysis revealed 139 deregulated genes, of which 104 were up- and 35 were downregulated (**Fig 3b, supplemental table 9**). GO-term and KEGG-pathway analysis revealed that the upregulated genes were linked to immune activation and phagocytosis (**Fig 3c; supplemental table 10**). In agreement with the *in vivo* data, we observed an increased expression of *Il1β*, *Tgfb1*, and *Tnfa*, which could be confirmed via qPCR (**Fig 3d; see also Fig S4c**). Next, we investigated phagocytosis, a key function of microglia that is altered during neuroinflammation³⁵. In a first approach we employed immortalized microglia (IMG) cells. Similar to the treatment with the lipopolysaccharide (LPS) commonly used to induce microglia activation, inhibition of miR-99b-5p caused an upregulation of proinflammatory cytokines and increased phagocytosis as measured via the uptake of fluorescent latex beads (**Fig S5**). Encouraged by these data we performed similar experiments in primary microglia isolated from the mouse PFC. In line with the data obtained in IMG cells, treatment of primary microglia with anti-miR-99b LNAs significantly increased phagocytosis (**Fig 3e**).

Aberrant microglia activity can have detrimental effects on neuronal plasticity³⁶. To test whether the reduced expression of miR-99b-5p in microglia could affect neuronal plasticity, we performed a co-culturing experiment. Primary microglia were first treated with sc-control or anti-miR-99b LNAs for 48 h before being harvested and transferred to cortical neuronal cultures (**Fig 3f**). RNA was isolated from these co-cultures after 48 h and subjected to RNA-seq. Differential expression analysis revealed 366 deregulated genes (155 upregulated and 211 downregulated genes, adjusted p value < 0.05, log2FC +/- 0.1); **Fig. 3g, supplemental table 11**). GO term analysis of the upregulated genes revealed neuroinflammatory processes, neuron death, neuron apoptotic processes as well as synaptic pruning (**Fig 3h, supplemental table 12_UP**), while downregulated genes were associated with processes indicating loss of synaptic function such as regulation of axon extension or synapse organization (**Fig 3h, supplemental table 12_DOWN**).

These data are in agreement with our previous findings suggesting that loss of miR-99b-5p increases inflammatory processes in microglia. More importantly, the data suggest that microglia lacking miR-99b-5p may have detrimental effects on synaptic function when co-cultured with cortical neurons. It is particularly interesting that synaptic pruning is detected as a major process increased in the co-

cultures, since synaptic pruning has been linked to SZ³⁶. In line with this, key factors of the complement system known to drive pathological synaptic pruning were increased in primary microglia treated with anti-miR-99b, as well as in the corresponding co-cultures and also in the postmortem human prefrontal cortex of schizophrenia patients (**Fig S6**). When we analyzed the number of dendritic spines, we observed that spine density was significantly reduced in neurons co-cultured with microglia that had received anti-miR-99b, when compared to cultures treated with corresponding control microglia (**Fig 3 i**).

miR99b-5p control neuroinflammation via the regulation of Zbp1

The three RNAseq datasets obtained from the PFC of mice, primary microglia and the co-cultures consistently show that knockdown of miR-99b-5p increases the expression of genes linked to inflammatory processes. Many of the gene expression changes likely represent secondary effects. To better understand the mechanisms by which miR-99b-5p controls neuroinflammation, we aimed to identify direct targets of miR-99b-5p (**supplemental table 13**). When we analyzed the RNA-seq data obtained from the PFC (see Fig 2), we identified 13 out of 113 genes as potential mRNA targets of miR99b-5p (**Fig 4A**). GO term analysis was performed for the 13 genes and revealed that they are linked to inflammatory processes including type I interferon signaling (**Fig S7, supplemental table 14**), linked to schizophrenia^{37 38}. Seven of these genes were also upregulated in primary microglia treated with anti-miR-99b, and among them were key regulators of inflammatory processes such as *Stat1* which was found to be hyperactive in blood samples of SZ patients³⁹. A gene that specifically caught our attention was *Zbp1* because the corresponding protein - also known as the DNA-dependent activator of interferon regulatory factors (*Dai*) - is a key regulator of pro-inflammatory processes that result in the activation of inflammatory caspases and the induction of *Il1β*²⁷. Thus, *Zbp1* represented a rather upstream factor in the inflammatory cascade. On this basis, we speculated that the regulation of *Zbp1* could be a key mechanism by which miR-99b-5p regulates inflammatory processes and may contribute to the pathogenesis of SZ when it is increased.

First, we performed a luciferase assay to directly test the regulation of *Zbp1* by miR-99b-5p. We used the renilla dual luciferase reporter vector harboring the *Zbp1*-3'UTR. Co-transfection of this vector with miR-99b-5p LNAs significantly reduced the luciferase activity (**Fig 4b**), but this was not the case when scramble control LNAs were used (**Fig 4b**). Moreover, we observed that ZBP1 protein levels were significantly increased in primary microglia treated with anti-miR-99b (**Fig 4c**). These data show that miR-99b-5p can directly regulate *Zbp1* levels.

On this basis we decided to investigate whether the inflammatory phenotypes induced in response to decreased miR-99b-5p levels depend on *Zbp1*. So far, we have found that decreased levels of miR-99b-5p lead to enhanced phagocytosis and increased expression of pro-inflammatory cytokines such as *IL1 β* which has been associated with *ZBP1* activity⁴⁰. Another important step in ZBP1-mediated orchestration of inflammation is the activation of pro-inflammatory caspases^{41 42}, and therefore we examined whether reduced miR-99b-5p levels would also affect the activity of pro-inflammatory caspases. Indeed, when primary microglia were treated with anti-miR-99b, caspase activity was significantly increased when compared to that in cells treated with sc-control LNAs (**Fig. 4d**). Similar findings were obtained when protein lysates isolated from the PFC of mice injected with either anti-miR-99b or sc-control LNAs were analyzed for caspase activity (**Fig. 4e**).

To test whether the miR-99b-5p-mediated increase in caspase activity, *IL-1 β* expression and phagocytosis depends on *Zbp1*, we treated primary microglia with either anti-miR-99b alone or in combination with an anti-sense oligonucleotide (ASO) targeting *Zbp1* (*Zbp1*-ASO). In agreement with our previous observation, anti-miR-99b treatment increased caspase activity. This effect was ameliorated in microglia treated with anti-miR-99b and *Zbp1*-ASO (**Fig 4f**). Similar observations were made when we analyzed *IL1 β* expression (**Fig. 4g**) and phagocytosis (**Fig 4h**). These data suggest that ZBP-1 plays an important role in mediating the neuroinflammatory processes downstream of miR-99b-5p.

We performed parallel experiments in human iPSC-derived microglia. Similar to the mouse data, administration of anti-miR-99b increased caspase activity (**Fig 4i**), *IL-1 β* expression (**Fig 4j**) and phagocytosis (**Fig 4k**) when compared to human iPSC-derived microglia treated with sc-control LNAs. These effects were attenuated when anti-miR-99 LNAs were co-administered with *Zbp1*-ASOs (**Fig 4i-k**). These data suggest that in human microglia, miR-99b-5p also controls neuroinflammatory processes via the regulation of *Zbp-1* expression. In line with this interpretation, *IL1 β* and *Zbp1* mRNA levels were increased in postmortem human brain samples from SZ patients and controls (**Fig. S8a**).

To determine whether knockdown of *Zbp1* would also mitigate the effect of anti-miR-99b treatment on SZ-like behavior in mice, we injected either anti-miR-99b alone or in combination with *Zbp1*-ASOs into the PFC of mice before subjecting the animals to behavior testing. Mice injected with sc-control LNAs served as controls. The corresponding data revealed that *Zbp1* knockdown rescues anti-miR-99b-mediated impairment of PPI (**Fig. S8**).

Our findings suggest that reduced miR-99b-5p levels in microglia contribute to the pathogenesis of schizophrenia via the regulation of *Zbp1*-controlled neuroinflammation. Therefore, miR-99b-5p may constitute a novel biomarker for SZ, while targeting miR-99b-5p and/or ZBP1 might represent an effective SZ treatment

Discussion

In this study we combined the analysis of blood samples and postmortem brain tissue to identify miRs involved in the pathogenesis of SZ. Using WGCNA as well as differential expression analysis in blood samples, we identified several miRs that differed between patients and controls and were significantly correlated with SZ phenotypes. GO term analysis of the confirmed target genes of these miRs hinted at a number of molecular processes of which pathways linked to immune function were overrepresented. Such a GO term analysis based on miR target genes is, of course, not ultimately conclusive but our observation is in agreement with previous studies showing that neuroinflammation plays a role in the pathogenesis of SZ^{43 44}. To further refine the identification of miRs linked to SZ we also performed a differential expression analysis of the small RNA seq data obtained from blood as well as from postmortem brain tissue of SZ patients and controls. We eventually identified five candidate miRs, miR-101-3p, miR-378a-3p, miR-21-5p, miR-192-5p and miR-103a-3p, that were increased in the blood and brain of SZ patients. All of these miRs have been implicated brain and non-brain diseases. For example, knock-down of miR-101-3p in the hippocampus impairs learning in mice⁴⁵ while increased circulating levels of miR-101-3p have been observed in patients suffering from autism⁴⁶, attention-deficit hyperactivity disorder⁴⁷ but also diabetes^{48 49} or cancer⁵⁰. MiR-378a-3p has been associated with cerebral ischemia⁵¹ is increased in blood samples of Down syndrome patients⁵² and was reported to be part of a blood-miR signature that can distinguish Alzheimer's disease patients from control⁵³. miR-21-5p was found to be increased in blood samples of SZ patients²⁹, while antipsychotic treatment is correlated with decreased miR-21-3p expression⁵⁴. Moreover, miR-21-3p was altered in blood samples of patients suffering from bipolar disease⁵⁵. However, altered miR-21-3p has also been observed in various other diseases and is for example increased in patients with lung cancer⁵⁶. Several studies have linked miR-192-5p to cognitive function and depression. For example, miR-192-5p was decreased in the blood AD patients upon aerobic exercise⁵⁷ and was altered in the brains of patients suffering from major depressive disorder⁵⁸, while increasing the levels of miR-192-5p in a mouse model for depression ameliorated cognitive impairments⁵⁹. Finally, altered blood levels of miR-103-3p have been linked to childhood traumatization and depression⁶⁰ as well as Autism⁶¹.

Four miRs, miR-500a-3p, miR-501-3p, miR-221-5p and miR-99b-5p, that all originated from the ME_Turquoise co-expression module which was downregulated in SZ patients and significantly correlated to SZ phenotypes, were also decreased in the postmortem brains of SZ patients. A recent study identified miR-501-3p as a schizophrenia-associated miR as it was found to be decreased in blood samples of monozygotic twins discordant for SZ²¹. The authors went on to show that loss of miR-501-3p in mice leads to SZ-like phenotypes, a finding that was linked to miR-501-3p-mediated

regulation of *metabotropic glutamate receptor 5* expression in the cortex. These data are in agreement with our observation that miR-501-3p was decreased in SZ patients of the PsyCourse study as well as in the postmortem brains of SZ patients. As to the other 3 miRs, there are thus far no data on the role of miR-500a-3p in the CNS, and while miR-221-5p has recently been linked to the regulation of synaptic processes⁶², there are still also no data on the role of miR-221-5p in SZ. As regards to miR-99b-5p, no functional data are available on its role in the CNS, and no report has as yet implicated this miR in the pathogenesis of SZ.

In summary, we have discovered miRs that have already been linked to the pathogenesis of SZ or other brain diseases, as well as miRs that have not been extensively studied so far. These data suggests that our approach may provide a viable means to detect novel SZ-associated miRs.

To test this hypothesis, we decided to investigate miR-99b-5p that was part of the ME_Turquoise co-expression module but was also decreased in the postmortem brain of SZ patients as well as in the blood of SZ patients, when the data was analyzed via differential expression. Moreover, essentially nothing was known about the role of miR-99b-5p in the adult brain. Inhibiting miR-99b-5p in the prefrontal cortex of mice led to impaired PPI and increased anxiety. PPI is impaired in SZ patients and in mouse models for SZ^{32 33}. Furthermore, increased anxiety is a phenotype often observed in SZ patients³⁰, suggesting that reduced miR-99b-5p levels are indeed linked to the development of SZ-like phenotypes. Nevertheless, these data cannot establish a clearly causal link between reduced miR-99b-5p expression and the pathogenesis of SZ in humans, since no animal model can fully recapitulate the complex processes in human patients due to functional and structural differences in cortical anatomy^{63 64}.

However, that miR-99b-5p is involved in the pathogenesis in SZ is further underscored by the results of our molecular analysis. RNA-seq analysis of the prefrontal cortex of mice revealed that inhibition of miR-99b-5p mainly led to an increased expression of genes, which is in agreement with the established action of miRs in controlling mRNA levels. Furthermore, the upregulated genes were almost exclusively related to immunity pathways in microglia, a process which has been linked to the pathogenesis of SZ by various means. For example, altered microglia have been observed in postmortem brain samples of SZ patients⁶⁵. In addition, epidemiological data demonstrated a correlation between immune diseases and SZ⁶⁶, while several neuroimaging studies reported an increase in activated microglia in the brains of SZ patients^{67 68}. Finally, studies in animal models have implicated aberrant microglia activation with the onset of SZ-like phenotypes^{69 70}. While miR-99b-5p has not been studied in microglia so far, these data are in line with previous reports demonstrating a role of the miR-99b in the modulation of inflammatory responses. For example, miR-99b levels are decreased in tumor-associated macrophages and re-expression of miR-99b attenuates tumor growth

⁷¹. Furthermore, inhibition of miR-99b in dendritic cells significantly elevated the levels of proinflammatory cytokines including *Il1 β* and *Tnfa* ⁷². These findings are in agreement with our data showing that inhibition of miR-99b-5p in the prefrontal cortex of mice increased the expression of pro-inflammatory cytokines including *Il1 β* and *Tnfa* in microglia that we had isolated from the brains of these mice via FACS. A strong upregulation of genes linked to inflammatory processes, including the upregulation of *Il1 β* and *Tnfa*, was also observed when miR-99b-5p was inhibited in IMG cells or primary microglia. This is interesting since increased *Il1 β* and *Tnfa* levels have been repeatedly reported in SZ patients ⁷³ and may offer novel therapeutic avenues. For example, inhibition of TNF α was recently shown to ameliorate disease phenotypes in different mouse models of SZ ⁷⁰.

Aberrant microglia activation can affect neuronal function via synaptic pruning, a process that is based on the phagocytic activity of microglia ⁷⁴. We observed that inhibition of miR-99b-5p in IMG cells and in primary microglia increased their phagocytic activity. Moreover, cortical neurons co-cultured with microglia that were treated with anti-miR-99b oligonucleotides displayed differentially expressed genes, of which the downregulated genes were linked to GO terms such as synapse assembly, regulation of synaptic plasticity or dendritic spine organization. As for the upregulated genes, the most significant GO term was synapse pruning. Since our data also revealed that neurons co-cultured with anti-miR-99b-treated microglia indeed displayed a reduced number of dendritic spines, our findings suggest a scenario in which reduced levels of miR-99b-5p lead to an upregulation of proinflammatory processes in microglia, which eventually impacts on synaptic structure. This interpretation is in agreement with previous reports suggesting that aberrant microglia activation leads to pathological synaptic pruning, which in turn leads to plasticity defects which could drive the pathogenesis of SZ ^{36 75}. Notably, the increased expression of several complement factors in microglia have been implicated in this process ⁷⁶. In line with these data, we observed increased expression of key complement factors in primary microglia and in corresponding microglia/neuron co-cultures in which miR-99b-5p was inhibited, as well as in postmortem brain samples from SZ patients. In summary, these findings provide a plausible mechanism on how reduced levels of miR-99b-5p can contribute to the pathogenesis of SZ, namely the induction of a pro-inflammatory response associated with synaptic pruning. Nevertheless, we cannot exclude that additional mechanisms within microglia or other neural cells play a role.

MiRs mediate their biological action by controlling the expression of specific target mRNAs. Our data showed that within microglia, miR-99b-5p controls the expression of the *Zbp1* gene that plays an important role in the innate immune response ²⁷. ZBP1 acts as sensor for Z-DNA/Z-RNA and controls inflammatory pathways such as type I interferon-signaling and other pathways, eventually leading to the upregulation of various pro-inflammatory cytokines including e.g. the induction of *Il1 β* ^{77 78 40}.

These data suggest that reduced levels of miR-99b-5p in microglia contribute to SZ-like phenotypes because the tight control of *Zbp1* levels is lost. In line with this interpretation, we demonstrated that the administration of *Zbp1*-ASO rescues the effects of anti-miR-99b treatment on SZ-like phenotypes in mice as well as in the corresponding cellular alterations observed in primary microglia from mice as well as in microglia derived from human iPSCs. Interestingly, the cellular processes we find to be affected by altered miR-99b-5p and *Zbp1* levels have also been implicated in other brain diseases. Thus, it will be important to investigate the role of miR-99b-5p and *Zbp1* in other neuropsychiatric diseases. Moreover, aberrant microglia activation and synaptic pruning is observed in neurodegenerative diseases such as Alzheimer's disease ⁷⁹, and ZBP1 also controls the NLRP3 inflammasome ⁷⁸, a key regulator of neuroinflammatory phenotypes in Alzheimer's disease ⁸⁰. In this context it is interesting to note that one study found decreased miR-99b-5p levels in plasma samples obtained in a mouse model of Alzheimer's disease when measured at 6 and 9 months of age, while increased levels were reported in older mice ⁸¹. These data might underscore the need for further study as to the role of *miR-99b-5p* and *Zbp1* in microglia obtained from wild type mice as well as mouse models for neuropsychiatric or neurodegenerative diseases at different ages. Indeed, it is well established that microglia undergo age-dependent functional changes and even differ between brain regions ^{82 83}.

There are other questions we could not address within the scope of this manuscript. It will for example be interesting to investigate the other candidate miRs we found in addition to miR-99b-5p. Similarly, it will be important to study the potential miR-99b-5p targets we found in addition to *Zbp1* in the context of SZ. Another question relates to the mechanisms that underlie the downregulation of miR-99b-5p in SZ patients. In future projects it will be interesting to test for example whether miR-99b-5p is altered in SZ mouse models that are based on either genetic or environmental risk factors such as early life stress. In addition, it will be important to identify the source of elevated miR-99b-5p levels in blood samples of SZ patients. It is known that miRs can be transported from the brain to the periphery within exosomes ^{84 25}, and recent studies reported the isolation of microglia-derived exosomes from human blood ⁸⁵. While this approach is not undisputed, it will be interesting to apply such methods to the PsyCourse Study, which is, however, beyond the scope of the current work. Although our findings that miR-99b-5p is decreased in the brain and the blood of SZ patients support the idea that the changes in blood may reflect corresponding changes in the brain, we cannot conclusively answer this question at present. Rather, we suggest that the analysis of miR-99b-5p levels in blood may eventually help stratify patients for treatment, including novel approaches based on RNA therapeutics towards miR-99b-5p or *Zbp1*.

In conclusion, in the present study we identify a miR-99b-5p-*Zbp1* pathway in microglia as a novel mechanism that likely contributes to the pathogenesis of schizophrenia. Our data also suggest that strategies to increase the levels of miR-99b-5p or inhibit *Zbp1*, for example via ASOs, could serve as novel therapeutic strategies for treating SZ patients.

Material and Methods

Human subjects:

All experiments involving human data were approved by the relevant Ethics committees (see Budde et al.). Informed written consent was obtained for all subjects. Blood samples (PAXgene Blood RNA Tubes; PreAnalytix, Qiagen) and behavioral data (supplemental table 1) of control and schizophrenia patients were obtained from participants of the PsyCourse Study²⁶. Psychiatric diagnoses were confirmed using the Diagnosis and Statistical Manual of Mental Disorders Fourth Edition (DSM-IV) criteria. Control subjects were screened for psychiatric disorders using parts of the structured clinical interviews for mental disorders across the lifespan (MINI-DIPS). All subjects were assessed for psychiatric symptoms through a battery of standard tests including the Positive and Negative Syndrome Scale (PANSS), the Global Assessment of Functioning Scale (GAF), and the Beck depression inventory (BDI-II).

Post-mortem human brain samples:

Postmortem tissue samples (prefrontal cortex A9&24) from controls (n = 17; 5 females & 12 males; age = 62.3 ± 18.9 years, PMD = 19.7 ± 6.7 h) and schizophrenia patients (n = 13; 5 females & 8 males; age 57.7 ± 16.8 years, PMD = 21 ± 6.4 h) were obtained with ethical approval and upon informed consent from the Harvard Brain Tissue Resource Center (Boston, USA). RNA was isolated using Trizol as described in the manufacturer protocol using the Directzol RNA isolation kit (Zymo Research, Germany). RNA concentration was determined by UV measurement. RNA integrity for library preparation was assessed using an RNA 6000 NanoChip in a 2100 Bioanalyzer (Agilent Technologies).

High throughput small RNAome sequencing:

Small RNAome libraries were prepared with total RNA according to the manufacturer's protocol with NEBNext® small RNA library preparation kit. All human subject small RNAome libraries were prepared with 150 ng of total RNA. Briefly, total RNA was used as starting material, and the first strand of cDNA was generated, followed by PCR amplification. Libraries were pooled and PAGE was run for size selection. For small RNAome, ~150 bp band was cut and used for library purification and quantification. A final library concentration of 2 nM was applied for sequencing. The Illumina HiSeq

2000 platform was used for sequencing and was performed using a 50-bp single read setup. Illumina's conversion software bcl2fastq (v2.20.2) was used for adapter trimming and converting the base calls in the per-cycle BCL files to the per-read FASTQ format from raw images. Demultiplexing was carried out using Illumina CASAVA 1.8. Sequencing adapters were removed using cutadapt-1.8.1. Sequence data quality was evaluated using FastQC (<http://www.bioinformatics.babraham.ac.uk/projects/fastqc/>). Sequencing quality was determined by the total number of reads, the percentage of GC content, the N content per base, sequence length distribution, duplication levels, overrepresented sequences and Kmer content.

Data processing, QC, and Differential expression (DE) analysis:

Sequencing data was processed using a customized in-house software pipeline. Quality control of raw sequencing data was performed by using FastQC (v0.11.5). The quality of miRNAs reads was evaluated by mirtrace (v1.0.1). Reads counts were generated using TEs small (v0.4.0) which uses bowtie (v1.1.2) for mapping. Reads were aligned to the Homo_sapiens GRCh38.p10 genome assembly (hg38). The miRNA reads were annotated using miRBase. Read counts were normalized with the DESeq2 (v1.26.0) package. Unwanted variance such as batch effects, library preparation effects, or technical variance was removed using RUVSeq for all data (v1.20.0; k = 1 was used for factors of unwanted variation). DESeq2 was utilized for differential expression analysis and adjustment of confounding factors. In the DESeq2 model, the PsyCourse data were corrected for sex, age and medication in DESeq2. Volcano plots were plotted with the R package EnhancedVolcano (v1.4.0).

WGCNA analysis:

microRNAome co-expression module analysis was carried out using the weighted gene co-expression network analysis (WGCNA) package (version 1.61) in R⁸⁶. We first regressed out age, gender, and other latent factors from the sequencing data, and after that, normalized counts were log (base 2) transformed. Next, the transformed data were used to calculate pairwise Pearson's correlations between microRNAs and define a co-expression similarity matrix, which was further transformed into an adjacency matrix. Next, a soft thresholding power of 8 was chosen based on approximate scale-free topology and used to calculate pairwise topological overlap between microRNAs in order to construct a signed microRNA network. Modules of co-expressed microRNAs with a minimum module size of 10 were later identified using cutreeDynamic function with the following parameters: method = "hybrid", deepSplit = 4, pamRespectsDendro = F, pamStage = T. Closely related modules were merged using a dissimilarity correlation threshold of 0.25. Different modules were summarized as a network of modular eigengenes (MEs), which were then correlated with the different psychiatric symptoms

and functionality variables (e.g., PANSS, GAF etc). The module membership (MM) of microRNAs was defined as the correlation of microRNA expression profile with MEs, and a correlation coefficient cutoff of 0.5 was set to select the module specific microRNAs. The Pearson correlation of MEs and psychiatric symptoms and functionality variable was plotted as a heat map.

Enriched gene ontology and pathways analysis:

To construct the Gene Regulatory network (GRN) for miRNA-target genes we retrieved validated microRNA targets from miRTarBase (v 7.0) (<http://mirtarbase.mbc.nctu.edu.tw/>). microRNA target genes were further filtered based on the expression in the brain. Brain-enriched expression was examined using the Genotype-Tissue Expression (GTEx) database. (GTEx Consortium). To identify the biological processes and their pathways in the miRNA-target genes, the ClueGO v2.2.5 plugin of Cytoscape 3.2.1 was used⁸⁷. In the ClueGo plugin⁸⁸ a two-sided hypergeometric test was used to calculate the importance of each term and the Benjamini-Hochberg procedure was applied for the P value correction. KEGG (<https://www.genome.jp/kegg/>) and Reactome (<https://reactome.org/>) databases were used for the pathway analysis. To construct GRN for significantly deregulated mRNAs, the ClueGO v2.2.5 plugin of Cytoscape 3.2.1 was used. Biological processes (BP) and pathways with adjusted p value < 0.05 were selected for further analysis. For further analysis, cellular metabolism and cancer-related biological processes were omitted. Key BPs with low levels of GOLevel (because terms at lower levels are more specific and terms higher up are more general) were further considered for data presentation and interpretation.

microRNA and mRNAs lipid nanoparticles preparation:

miR99b-5p inhibitor sequences were used to decrease the expression of miR99b-5p. To decrease the expression of mRNAs, anti-sense oligos (ASO) were employed. ASOs, inhibitor and negative control sequences were purchased from Qiagen. MicroRNA inhibitor, or ASOs lipid nanoparticle (LNP) formulation, was achieved using a proprietary mixture of lipids containing an ionizable cationic lipid, supplied as Neuro9™ siRNA Spark™ Kit (5 nmol). The miRNA inhibitor or ASOs were encapsulated using a microfluidic system for controlled mixing conditions on the NanoAssemblr™ Spark™ system (Precision Nanosystems, Canada). The experiments were performed as described in the manufacturer's protocol. Briefly, 5 nmol lyophilized microRNA inhibitor or ASOs were dissolved in formulation buffer 1 (FB1) to a final concentration of 2 nmol. This solution was further diluted to a final concentration of 930 ug/mL. Formulation buffer 2 (FB 2), microRNA inhibitor/ASOs in FB1, and lipid nanoparticles were added to the cartridge and encapsulated using the NanoAssembler Spark system.

545

546 *Animals*

547 C57BL/6J mice were purchased from Janvier and housed in an animal facility with a 12-h light–dark
548 cycle at constant temperature (23 °C) with *ad libitum* access to food and water. Animal experiments
549 complied with relevant ethical regulations and were performed as approved by the local ethics
550 committee. All experiments were performed with 3 months old male mice. Pre-frontal cortex (PFC)
551 region was dissected on day five after stereotaxic surgery for RNA-seq-based experiments.

552

553 *Stereotaxic surgery:*

554 For intracerebral stereotaxic injections of LNPs in the PFC, 3-month-old mice were anesthetized with
555 Rompun 5mg/kg and Ketavet 100mg/kg. After application of local anesthesia to the skull, two small
556 holes were drilled into the skull. Mice then received a bilateral injection of LNPs of microRNA
557 inhibitor/negative control or ASOs (dose: 0.15 ug/mL for microRNA inhibitor/negative control; dose:
558 0.3 ug/mL for ASO+ microRNA inhibitor mix). LNPs were injected with a rate of 0.3 µl/min per side.
559 Only 0.9 ul of LNPs were injected per hemisphere (0,5 µl/min). After surgery, all mice were monitored
560 until full recovery from the anesthesia and housed under standardized conditions.

561

562 *Behavioral phenotyping:*

563 The open field test was performed to evaluate locomotory and exploratory functions. Mice were
564 placed individually in the center of an open arena (of 1 m length, 1 m width, and side walls 20 cm
565 high). Locomotory activity was recorded for 5 min using the VideoMot2 tracking system (TSE Systems).
566 The elevated plus maze test was used to evaluate basal anxiety. Mice were placed individually in the
567 center of a plastic box consisting of two open and two walled closed arms (10 × 40 cm each, walls 40
568 cm high). Their behavior was recorded for 5 min using the VideoMot2 system. Time spent in open
569 versus closed arms was measured to assay basal anxiety phenotype. Prepulse inhibition (PPI) was
570 performed to test the acoustical startle response (ASR). ASR was completed in an enclosed sound-
571 attenuated startle box from TSA Systems. In brief, mice were placed individually inside a cage attached
572 with a piezoelectric transducer platform in a sound-attenuated startle cabinet. These sensory
573 transducers converted the movement of the platform induced by a startle response into a voltage
574 signal. Acoustic stimuli were executed through speakers inside the box. The mice were given 3 min to
575 habituate at 65 dB background noise and their activity was recorded for 2 min as baseline. After the
576 baseline activity recording, the mice were tested to six pulse-alone trials, at 120-dB startle stimuli
577 intensity for a duration of 40 ms. PPI of startle activity was measured by conducting trials for pre-pulse
578 at 120 dB for 40 ms or preceding non-startling prepulses of 70, 75, 80, 85, 90 dB.

RNA isolation:

Humans: PAXgene Blood RNA Tubes (PreAnalytix/Qiagen) were stored at -80°C. For RNA isolation, the tubes were thawed and incubated at room temperature overnight. RNA was extracted according to the manufacturer's protocol using PAXgene Blood RNA Kits (Qiagen). RNA concentrations were measured by UV measurement. RNA integrity for library preparation was determined by analyzing them on an RNA 6000 NanoChip using a 2100 Bioanalyzer (Agilent Technologies).

Mice: The mice were sacrificed by cervical dislocation on day five after stereotaxic surgery. Unilateral PFC region was collected and immediately frozen in liquid nitrogen and later stored at -80°C until RNA isolation. Total RNA was isolated using the trizol method as described by the manufacturer's protocol using the Directzol RNA isolation kit (Zymo Research, Germany). The RNA concentration was determined by UV measurement. RNA integrity for library preparation was assessed using a Bioanalyzer (Agilent Technologies).

RNA sequencing:

Total RNA was used for the library preparation using the TrueSeq RNA library prep kit v2 (Illumina, USA) according to the manufacturer's protocol. 500 ng RNA was used as starting material. The quality of the libraries was assessed using the Bioanalyzer (Agilent Technologies). Library concentration was measured by Qubit™ dsDNA HS Assay Kit (Thermo Fisher Scientific, USA). Multiplexed libraries were directly loaded onto a HiSeq2000 (Illumina) with 50 bp single read setup.

The sequencing data were processed using a customized in-house software pipeline. Illumina's conversion software bcl2fastq (v2.20.2) was employed for adapter trimming and converting the base calls in the per-cycle BCL files to the per-read FASTQ format from raw images. Quality control of raw sequencing data was carried out using FastQC (v0.11.5)(<http://www.bioinformatics.babraham.ac.uk/projects/fastqc/>). Reads were aligned using the STAR aligner (v2.5.2b) and read counts were generated using featureCounts (v1.5.1). The mouse genome version mm10 was utilized.

Publicly available datasets:

Various publicly available datasets were used in this study to explore cell type-specific expression of differentially expressed genes. Published single cell data⁸⁹ were utilized to explore neuron-, astrocyte-, and microglia-specific expression of genes. Immunome-related genes were retrieved from the Immunome database. The Immune Response In Silico (IRIS) dataset was used to explore immunity-related genes^{90 91}

Primary microglia cultures:

Primary mouse microglia cell cultures were prepared as previously described for wild-type pups⁹². In brief, newborn mice (P1 pups) were used to prepare mixed glia cultures. Cells were grown in DMEM (Thermo Fisher Scientific) with 10% FBS, 20% L929 conditioned medium and 100 U ml⁻¹ penicillin–streptomycin (Thermo Fisher Scientific). Microglia were collected 10–12 days after cultivation by shake off, counted and plated in DMEM supplemented with 10% FBS, 20% L929 conditioned medium and 100 U ml⁻¹ penicillin–streptomycin. The microglia were shaken off up to two times.

Ex-vivo isolation of microglia:

PFC regions were dissected, mechanically dissociated and digested for 15 minutes with liberase (0.4 U/mL; Roche) and DNase I (120 U/mL; Roche) at 37°C. Subsequently, the cell suspension was passed through a 70 µm cell strainer. Myelin debris was eliminated by the Percoll density gradient. Single cell suspension was labeled by using anti-mouse CD45 BV 421 (Clone 30-F11, Biolegend) and CD11b FITC (Clone M1/70, Biolegend). Antibody-labeled CD45^{low} CD11b⁺ microglial cells were sorted using a FACS Aria 4L SORP cell sorter (Becton Dickinson) The purity of the sorted microglial cells was above 90%.

Primary neuronal culture:

Primary neuronal cultures were prepared from E17 pregnant mice of CD1 background (Janvier Labs, France). Briefly, mice were sacrificed and the brains of embryos were taken out, meninges removed, and the cortex dissected out. The cortexes were washed in 1× PBS (Pan Biotech, Germany). Single-cell suspensions were generated by incubating them with trypsin and DNase before careful disintegration. One hundred and thirty thousand cells per well were plated on poly-D-lysine-coated 24-well plates in Neurobasal medium (Thermo Fisher Scientific, Germany) supplemented with B-27 (Thermo Fisher Scientific, Germany). Primary cortical neurons were used for experiments at DIV10–12.

Cell lines

All human iPSCs used in this study are commercially available and reported to be derived from material obtained under informed consent and appropriate ethical approvals.

Differentiation of microglia from induced pluripotent stem cells:

Human induced pluripotent stem cells lines (hiPSCs) (Cell line IDs: KOLF2.1J⁹³ were obtained from The Jackson Laboratory; BIONi010-C and BIONi037-A were both from the European bank for Induced Pluripotent Stem Cells) were differentiated to microglia as previously described⁹⁴. In brief, 3 x 10⁶

iPSCs were seeded into an Aggrewell 800 well (STEMCELL Technologies) to form embryoid bodies (EBs), in mTeSR1 and fed daily with medium plus 50 ng/ml BMP4 (Miltenyi Biotec), 50 ng/ml VEGF (Miltenyi Biotec), and 20 ng/ml SCF (R&D Systems). Four-day EBs were then differentiated in 6-well plates (15 EBs/well) in X-VIVO15 (Lonza) supplemented with 100 ng/ml M-CSF (Miltenyi Biotec), 25 ng/ml IL-3 (Miltenyi Biotec), 2 mM Glutamax (Invitrogen Life Technologies), and 0.055 mM beta-mercaptoethanol (Thermo Fisher Scientific), with fresh medium added weekly. Microglial precursors emerging in the supernatant after approximately 1 month were collected and isolated through a 40 μ m cell strainer and plated in N2B27 media supplemented with 100 ng/ml M-CSF, 25 ng/ml interleukin 34 (IL-34) for differentiation.

Quantitative PCR experiment:

cDNA synthesis was performed using the miScript II RT Kit (Qiagen, Germany) according to the manufacturer's protocol. In brief, 200 ng total RNA was used for cDNA preparation. HiFlex Buffer was used so that the cDNA could be used for both mRNA and microRNA quantitative PCR (qPCR). A microRNA-specific forward primer and a universal reverse primer were used for quantification. The U6 small nuclear RNA gene was employed as an internal control. For mRNA quantification, gene-specific forward and reverse primers were used. The relative amounts of mRNA were normalized against GAPDH. The fold change for each microRNA and mRNA was calculated using the $2^{-\Delta\Delta Ct}$ method¹⁸. The Light Cycler® 480 Real-Time PCR System (Roche, Germany) was used to perform qPCR.

Caspase 1 activation assay:

Caspase-Glo® 1 Inflammasome Assay (Promega, Germany) was used to detect caspase 1 activation as described in the manufacturer's protocol. In brief, microglia, treated with ASO/inhibitor or primed with LPS and stimulated with ATP, were seeded on opaque, flat-bottom 96-well plates (Cellstar, Germany) at 50,000 per well in 100 μ l DMEM supplemented with 10% FBS, 20% L929 conditioned medium and 100 U ml⁻¹ penicillin–streptomycin. 100 μ l of Caspase-Glo buffer was mixed with cell medium. Plates were incubated at room temperature for 1 h. Luminogenic caspase activity was measured using a FLUOstar Omega plate reader (BMG Labtech).

Microglia phagocytosis assay:

The microglia phagocytosis assay was performed as described¹⁹. Primary microglia cultures were plated at a density of 18×10^4 in poly-D-lysine-coated 24-well plates in DMEM supplemented with 10% FBS, 20% L929 conditioned medium and 100 U ml⁻¹ penicillin–streptomycin. Immortalized microglia (IMG) cultures were plated at a density 5×10^3 in poly-D-lysine-coated 24-well plates in DMEM

supplemented with 10% FBS, 1X Glutamine (Millipore), and 100 U ml⁻¹ penicillin–streptomycin. To evaluate phagocytosis, treated microglia were incubated with fluorescent latex beads of 1 µm diameter (green, fluorescent 496/519; Sigma-Aldrich) for 1 h at 37°C, rinsed, and fixed with 4% formaldehyde. Cells were stained using the Iba1 (CD68) antibody (1:500; Wako) and DAPI. A confocal microscope was used for imaging at a low magnification (10x). ImageJ was used to quantify fluorescent latex beads. Region of interests (ROIs) were selected as microglial cells outlined with the Iba1 immunostaining to quantify beads. An intracellular section of the cell was selected to assure engulfment of latex beads by microglia. Similar acquisition parameters were used for each individual experiment. The results were expressed as the percentage of phagocytic index (# of total engulfed beads in an image / # of total cells identified in an image; n = 13 independent experiments).

Synaptic pruning in primary microglia neural co-culture:

Primary cortical neurons were seeded at a density of 130,000 on poly-D-lysine-coated 13 mm coverslips in 24-well plates in Neurobasal medium supplemented with B-27. Primary cortical neurons were used for experiments at DIV10-12. Treated primary microglia cultures were harvested from T-75 flasks and 4000 cells were seeded to each neural culture well. Plates were kept at 37°C for three days. On the third day, the cells were washed and fixed with 4% PFA (Sigma Aldrich, Germany) and 100 mM NH₄Cl (Merck, Germany) respectively, at room temperature for 30 minutes. Next, the cells were washed in permeabilization and blocking buffer (0.1% Triton-X [Merck, Germany] + 3% bovine serum albumin (BSA) [AppliChem GmbH, Germany]) on a shaker. The cells were then incubated with primary antibodies for 1 hour at room temperature. The antibodies used included synaptophysin 1 (guinea pig, SySy), PSD-95 (rabbit, Cell Signaling.), and Iba1 (goat, Abcam). After incubation, the cells were washed in PBS and then incubated with a secondary antibody for 1 hour at room temperature. As secondary antibodies, Cy3 (donkey, anti- guinea pig, Jackson Imm.), Abberrior STAR 635p (goat, anti-rabbit) were used. Mowiol (Merck, Germany) and DAPI were used as a mounting medium. Images were taken with a multicolor confocal STED microscope (Abberrior Instruments GmbH, Göttingen, Germany). Analysis of colocalization of pre- and post-synaptic markers were performed using SynQuant plugins in Fiji (v 2.0.0).

Dendritic spine analysis:

As described above, primary cortical neurons and primary microglia were co-cultured and fixed with 4%PFA. Dendritic spines were labeled as described⁹⁵. In brief, the cells were aspirated and 2-3 crystals of Dil stain (Life Technologies-Molecular Probes) were added to each culture well and incubated on a shaker for 10 minutes at room temperature. Cells were washed with PBS until no crystals were visible

and incubated overnight at room temperature. On the following day, the cells were washed and mounted with Mowiol. For high-magnification images, a multicolor confocal STED microscope with a 60× oil objective was used. Spine density and total spine length were measured by using ImageJ.

Protein extraction of primary microglia:

Primary microglia cell lysates were used to detect ZBP1 in RIPA fractions. Primary microglia were seeded in a 6-well plate at a density of 1×10^6 in each well. Cells were collected in a RIPA buffer supplemented with 1× protease inhibitor. Samples were kept on ice for 15 minutes and vortexed every 5 minutes and then centrifuged at 5000 rpm for 15 minutes at 4°C before supernatants were transferred to a new tube and stored at −20°C. The protein concentration was measured using a BCA assay.

Immunoblot analysis:

For standard immunoblot analysis, 20 µg of samples were mixed with 1× Laemmli buffer (Sigma, Germany), heated for 5 min at 95°C and loaded onto 4–15% Mini-PROTEAN® TGX™ Precast Protein Gels (Bio-Rad, Germany). Proteins were transferred on nitrocellulose membranes and membranes were blocked with 5% BSA in PBS-Tween. Membranes were incubated with primary antibodies in 5% BSA in PBS-Tween. Fluorescent-tagged secondary antibodies (LI-COR) were used for visualization of proteins. Imaging was performed using a LI-COR ODYSSEY. HSP-70, GAPDH were used as a loading and run on the same gel.

Treatment of microglia:

Microglia activation by LPS was used as a positive control. For this, microglia cells were first primed with 100 ng/ml ultrapure LPS (E. coli 0111:B4, Invivogen) and then incubated at 37°C. After this, 5 mM ATP were added to the culture and incubated for 30 minutes. Caspase 1 assay and phagocytosis assay were performed from these cultures. For immunoblot, cell lysate was prepared. For miR99b-5p-related analysis, microglia were either treated for two days with miR99b-5p inhibitor/negative control or ASOs in T-75 after first harvesting or after harvesting cells were seeded in a 24-well culture plate.

Luciferase assay:

Seed sequences of miR-99b-5p and pairing 3'UTR sequences of Zbp1 were generated with TargetScan. Cloned 3'UTR sequence of Zbp1 and scrambles UTR were purchased from Gene Copoeia (<https://www.genecopoeia.com/product/mirna-target-clones/mirna-targets/>). UTR was cloned downstream to firefly luciferase of pEZX-MT06 Dual-Luciferase miTarget™ vector. The pEZX-MT06-

scrambled UTR or pEZX-MT06-Zbp1 3'UTR construct and miR99b-5p mimic or negative control were co-transfected into HEK293-T cells cultured in 24-well plates using EndoFectin™ Max Transfection Reagents (Gene Copoeia) according to the manufacturer's protocol. 48 hours after transfection, Firefly and Renilla luciferase activities were measured using a Luc-Pair™ Duo-Luciferase HS Assay Kit (for high sensitivity) (GeneCopoeia). Firefly luciferase activity and Renilla luciferase activity were normalized. The mean of luciferase activity and of Firefly/Renilla was considered for the analysis.

Statistical analysis:

Unless otherwise noted, statistical analysis was carried out with GraphPad Prism software version 8.0. Statistical measurement is shown as mean \pm SD. Each n represents a biological sample. Either a two-tailed unpaired t-test or a two-way ANOVA with Tukey's post hoc test were applied to analyze the data. Enriched gene ontology and pathway analysis was performed using Fisher's exact test followed by a Benjamini-Hochberg correction.

Conflict of interest

The authors declare no conflict of interest.

Acknowledgment

This work was supported by the following grants to AF: The DFG (*Deutsche Forschungsgemeinschaft*) priority program 1738, SFB1286, the EPIFUS project, Germany's Excellence Strategy - EXC 2067/1 390729940. FS was supported by the GoBIO project miRassay. Urs Heilbronner is supported by the European Union's Horizon 2020 Research and Innovation Programme (PSY-PGx, grant agreement No 945151) and the Deutsche Forschungsgemeinschaft (DFG, German Research Foundation, project number 514201724). LE is supported by the Studienstiftung des Deutschen Volkes and the International Max-Planck Research School for The Mechanisms of Mental Function and Dysfunction (IMPRS-MMFD). DKV is supported by grants from the Chan Zuckerberg Initiative Neurodegenerative's Challenge Network (2020-221779(5022) & 2021-235147). TS was supported by grants from

the *Deutsche Forschungsgemeinschaft* (DFG; SCHU 1603/4-1, 5-1, 7-1), the German Ministry of Education and Research (BMBF; 01EE1404H), and the Dr. Lisa Oehler Foundation (Kassel, Germany). PF was supported by a grant from the DFG (DFG; FA 241/16-1)

Figure legends

Figure 1: Identification of microRNAs that play a role in the pathogenesis of SZ. **a.** Experimental scheme. **b.** Violin plots showing the results of WGCNA analysis. Depicted is the comparison of the eigenexpression in of the 3 co-expression modules in SZ patients and in control, showing a decrease in SZ patients. **c.** Violin plots showing the results of WGCNA analysis. The eigenexpression of the 5 co-expression modules was higher in SZ patients than in controls (for b & c: unpaired t test; **P < 0.01, ***P < 0.001; ****P < 0.0001, a P value < 0.01 was considered as significant). **d.** Heat map showing the correlation of the eigenexpression of the co-expression modules shown in (a) and (b) with the corresponding clinical phenotypes. The numbers in each rectangle represent the correlation (upper number) and the corresponding p-value (lower number). A P value < 0.01 was considered as significant. **e.** Volcano plot depicting the results of the differential expression analysis when comparing SZ patients and controls shown in (a). **f.** Volcano plot demonstrating the results of the differential expression when comparing postmortem brain samples from SZ patients (n=13) and controls (n=17). **g.** Venn diagram comparing the microRNAs detected in blood samples when performing differential expression analysis (Blood DESEQ2_DE), the microRNAs of the ME_Turquoise and ME_Pink co-expression modules and the microRNAs differentially expressed when comparing postmortem brain tissue (brain_DE). miR-99b-5p is the only microRNA decreased in all comparisons. **h.** Heat map showing the correlation of miR-99b-5p expression levels to the clinical phenotypes for the individuals as analyzed in (a). The numbers in each rectangle represent the correlation (upper number) and the corresponding p-value (lower number).

Figure 2: Decreasing miR-99b-5p levels in the PFC of mice leads to SZ-like phenotypes and increases the expression of genes linked to microglia activation. **a.** Left panel: Experimental design. Right panel: Bar graph showing qPCR results for miR-99b-5p in tissue obtained from the PCF of mice 5 or 10 days after injection of anti-miR-99b or sc-control oligonucleotides. (n=4/group; ****P < 0.0001, unpaired t test). **b.** Bar graph showing the distance traveled in the open field test of mice injected to the PFC with either anti-miR-99b or sc-control oligonucleotides (n=10/group; unpaired t test. **c.** Bar graph showing the time spent in the center of the open field in mice injected to the PFC with either anti-miR-99b or sc-control oligonucleotides (n=10/group; *P < 0.05; unpaired t test). **d.** Bar graph showing the time spent in the open arms when an elevated plus maze test was performed in mice injected to the PFC

with either anti-miR-99b or sc-control oligonucleotides (n=10/group; *P < 0.05; unpaired t test). **e.** Bar graph showing the results of a PPI experiment of mice injected with either anti-miR-99b or sc-control oligonucleotides. PPI is impaired in anti-miR-99b injected mice (n=10/group) unpaired t test; *P < 0.05; **P < 0.01, ***P < 0.001; ****P < 0.0001). **f.** Bar graph showing the basic startle response among groups. **g.** Volcano plot showing the differentially expressed genes (upregulated in red, downregulated in blue) when RNA-seq was performed from the PFC of mice injected with either anti-miR-99b or sc-control oligonucleotides. Genes with log2-fold change \pm 0.5 and adjusted p value < 0.05 are highlighted. **h.** GO-term analysis of the upregulated genes found in (e). **i.** Heat maps showing the enrichment of the upregulated genes as determined in (e) in various datasets. Left panel shows that the upregulated genes are enriched for microglia-specific genes, while the downregulated genes are enriched for neuron-specific genes. The right panel shows that the upregulated genes are over-represented in 3 different databases for immune function-related genes. **j.** Bar graph showing the qPCR results of the *Il1 β* , *Tgfb1* and *Tnfa* genes in FACS-sorted microglia collected from the PFC of mice injected with anti-miR-99b or sc-control oligonucleotides. (n=4 or 5/group; unpaired t test; *P < 0.05). Error bars indicate SD.

Figure 3: Decreasing miR-99b-5p levels in microglia increases phagocytosis and reduces synapse number in cortical neurons **a.** Left panel: Experimental design. **b.** Volcano plot showing differential expressed genes when comparing microglia treated with anti-miR-99b or sc-control LNAs. Genes with statistical significance are highlighted. **c.** Bar chart showing the top GO terms represented by the up regulated genes shown in (b). **d.** Bar charts showing qPCR results for *Tgfb1*, *Il1 β* and *Tnfa* comparing microglia treated with anti-miR-99b or sc-control LNAs (n=6/group; unpaired t test; *P < 0.05; **P < 0.01, ****P < 0.0001). **e.** Bar chart showing the results of a phagocytosis assay performed in microglia treated with anti-miR-99b in comparison to cells treated with sc-control LNAs. The percentage of phagocytic index represents (# of total engulfed beads in an image / # of total cells identified in an image; n = 13 independent experiments; unpaired t test; *P < 0.01). **f.** Experimental scheme illustrating the co-culture experiment. **g.** Heat map showing the differentially expressed genes from the experiment described in (f). **h.** Plot showing the results of a GO term analysis for the up- and downregulated genes displayed in (g). **i.** Left panel: Representative image showing DIL dye staining to visualize dendritic spines in co-cultures as illustrated in (f). Scale bar 5 μ m. Right panel: Bar chart showing the statistical quantification of the data depicted in (i). Each dot represents a spine density for a dendritic segment. *P < 0.05; **P < 0.01, ***P < 0.001; ****P < 0.0001). Error bars indicate SD.

Figure 4: miR-99b-5p regulates neuroinflammatory phenotypes via *Zbp1* **a.** Venn diagram comparing the genes upregulated in the PFC of mice and in primary microglia when injected or treated with anti-miR99b vs. sc-control LNAs, respectively. The data is further compared to the identified 13 miR-99b-5p target mRNAs detected in the PFC dataset. The left panel shows the gene names of the 13 miR-99b-5p target mRNAs. Red indicates miR-99b-5p targets upregulated in the PCF and in primary microglia upon anti-miR-99b treatment. **b.** Bar graph showing the results of the luciferase assay. In comparison to sc-control LNAs, administration of miR-99b-5p mimic decreases luciferase activity when cells express the *Zbp1*-3'UTR. This effect is not observed when a control 3'UTR that does not bind miR-99b-5p is used. (n=6/group). The upper right panel shows the predicted binding of miR-99b-5p to the 3'UTR of *Zbp1*. **c.** Left panel: Representative immunoblot image showing ZBP1 levels in microglia treated with sc-control LNAs or anti-miR-99b. HSP70 was used as a loading control. Right panel: Bar graph showing the quantification of the data depicted in the left panel. n=4/group. **d.** Bar graph showing quantification of caspase activity in primary microglia treated with sc-control LNAs or anti-miR-99b (n=6/group). **e.** Bar graph showing quantification of caspase activity in protein lysates isolated from the PFC of mice injected with anti-miR-99b or sc-control (n=4/group). **f.** Bar graph showing quantification of caspase activity in primary microglia treated with either sc-control LNAs, anti-miR-99b or anti-miR-99b together with *Zbp1*-ASOs. (n=6/group). **g.** Bar graph showing qPCR results for *Il1 β* in primary microglia treated with either sc-control LNAs, anti-miR-99b or anti-miR-99b together with *Zbp1*-ASOs (n=6/group). **h.** Bar graph showing the results of a phagocytosis assay performed in primary microglia treated with either sc-control LNAs, anti-miR-99b or anti-miR-99b together with *Zbp1*-ASOs (n=16 independent experiments). **i.** Bar graph showing quantification of caspase activity in human iPSC-derived microglia treated with either sc-control LNAs, anti-miR-99b or anti-miR-99b together with *Zbp1*-ASOs (n=13-16 samples/group). **j.** Bar graph showing qPCR results for *IL1 β* in human iPSC-derived microglia treated with either sc-control LNAs, anti-miR-99b or anti-miR-99b together with *Zbp1*-ASOs (n=6/group). **k.** Bar graph showing the results of a phagocytosis assay performed in human iPSC-derived microglia treated with either sc-control LNAs, anti-miR-99b or anti-miR-99b together with *Zbp1*-ASOs. The percentage of phagocytic index represent (# of total engulfed beads in an image / # of total cells identified in an image; n = 9 independent experiments. Error bars indicate SD; unpaired t test; *P < 0.05; **P < 0.01, ***P < 0.001; ****P < 0.0001). RI: relative immunofluorescent,

References

- 1 Kessler, R. C., Chiu, W. T., Demler, O., Merikangas, K. R. & Walters, E. E. Prevalence, severity, and comorbidity of 12-month DSM-IV disorders in the National Comorbidity Survey Replication. *Arch. Gen. Psychiatry* **62** (2005).
- 2 Jaeschke, K. *et al.* Global estimates of service coverage for severe mental disorders: findings from the WHO Mental Health Atlas 2017. *Ment Health (Camb)* **21**, e27 (2021).
- 3 Nestler, E. J., Peña, C. J., Kundakovic, M., Mitchell, A. & Akbarian, S. Epigenetic Basis of Mental Illness. *Neuroscientist* **8** (2015).
- 4 Giegling, I. *et al.* Genetics of schizophrenia: A consensus paper of the WFSBP Task Force on Genetics. *World J Biol Psychiatry*. **18**, 492-505 (2017).
- 5 Robinson, N. & Bergen, S. E. Environmental Risk Factors for Schizophrenia and Bipolar Disorder and Their Relationship to Genetic Risk: Current Knowledge and Future Directions. *Front Genet.* **28**, 686666 (2021).
- 6 Samara, M. T. *et al.* Efficacy, Acceptability, and Tolerability of Antipsychotics in Treatment-Resistant Schizophrenia: A Network Meta-analysis. *JAMA Psychiatry* **73**, 199-210 (2016).
- 7 Spark, D. L., Fornito, A., Langmead, C. J. & Stewart, G. D. Beyond antipsychotics: a twenty-first century update for preclinical development of schizophrenia therapeutics. *Transl Psychiatry*. **7**, 147 (2022).
- 8 Ezkurdia, I. *et al.* Multiple evidence strands suggest that there may be as few as 19,000 human protein-coding genes. *Hum Mol Genet.* **23**, 5866-5878 (2014).
- 9 Damase, T. R. *et al.* The Limitless Future of RNA Therapeutics. *Front Bioeng Biotechnol.* **18**, 628137 (2021).
- 10 Feng, R., Patil, S., Zhao, X., Miao, Z. & Qian, A. RNA Therapeutics - Research and Clinical Advancements. *Front Mol Biosci.* **22**, 710738 (2021).
- 11 Rupaimoole, R. & Slack, F., J. . MicroRNA therapeutics: towards a new era for the management of cancer and other diseases. *Nat Rev Drug Discov.* **16**, 203-222 (2017).
- 12 Gurtan, A. M. & Sharp, P. A. The Role of miRNAs in Regulating Gene Expression Networks. *J Mol Biol pii*, Epub ahead of print (2013).
- 13 Bär, C. *et al.* Non-coding RNAs: update on mechanisms and therapeutic targets from the ESC Working Groups of Myocardial Function and Cellular Biology of the Heart. *Cardiovasc Res.* **116**, 1805-1819 (2020).
- 14 Fischer, A. Epigenetic memory: the Lamarckian brain. *EMBO J* **33**, 945-967 (2014).
- 15 Martins, H. C. & Schratt, G. MicroRNA-dependent control of neuroplasticity in affective disorders. *Transl Psychiatry.* **11**, 263 (2021).
- 16 Sakamoto, K. & Crowley, J. J. A comprehensive review of the genetic and biological evidence supports a role for MicroRNA-137 in the etiology of schizophrenia. *Am J Med Genet B Neuropsychiatr Genet.* **177**, 242-256 (2017).
- 17 Sargazi, S. *et al.* Functional Variants of miR-143 Are Associated with Schizophrenia Susceptibility: A Preliminary Population-Based Study and Bioinformatics Analysis. *Biochem Genet.* **60**, 868-881 (2022).
- 18 Roy, B. *et al.* Exploiting Circulating MicroRNAs as Biomarkers in Psychiatric Disorders. *Molecular diagnosis & therapy* **24**, 279-298 (2020).
- 19 Ghafouri-Fard, S. *et al.* Review on the Expression Pattern of Non-coding RNAs in Patients With Schizophrenia: With a Special Focus on Peripheral Blood as a Source of Expression Analysis. *Front Psychiatry.* **18**, 640463 (2021).
- 20 Tsermpini, E. E., Kalogirou, C. I., Kyriakopoulos, G. C., Patrinos, G. P. & Stathopoulos, C. miRNAs as potential diagnostic biomarkers and pharmacogenomic indicators in psychiatric disorders. *Pharmacogenomics J.* **22**, 211-222 (2022).
- 21 Liang, W. *et al.* Loss of schizophrenia-related miR-501-3p in mice impairs sociability and memory by enhancing mGluR5-mediated glutamatergic transmission. *Sci Adv* **8**, eabn7357 (2022).

933 22 Zampetaki, A., Willeit, P., Drozdov, I., Kiechl, S. & Mayr, M. Profiling of circulating microRNAs:
934 from single biomarkers to re-wired networks. *Cardiovascular research* **93**, 555–562. (2012).
935 23 Condrat, C. E. *et al.* miRNAs as Biomarkers in Disease: Latest Findings Regarding Their Role in
936 Diagnosis and Prognosis. *Cells* **9**, 276 (2020).
937 24 Jose, A. M. Movement of regulatory RNA between animal cells. *Genesis* **53**, 395–416 (2015).
938 25 Bayraktar, R., Van Roosbroeck, K. & Calin, G. A. Cell-to-cell communication: microRNAs as
939 hormones. *Mol Oncol.* **11**, 1673–1686. (2017).
940 26 Budde, M. *et al.* A longitudinal approach to biological psychiatric research: The PsyCourse
941 study. *Am J Med Genet B Neuropsychiatr Genet.* **180**, 89–102 (2018).
942 27 Kuriakose, T. & Kanneganti, T. D. ZBP1: Innate Sensor Regulating Cell Death and Inflammation.
943 *Trends Immunol.* **39**, 123–134 (2018).
944 28 Ermakov, E. A., Melamud, M. M., Buneva, V. N. & Ivanova, S. A. Immune System Abnormalities
945 in Schizophrenia: An Integrative View and Translational Perspectives. *Front Psychiatry.* **25**,
946 880568 (2022).
947 29 Liu, S. *et al.* Diagnostic value of blood-derived microRNAs for schizophrenia: results of a meta-
948 analysis and validation. *Scientific reports* **7**, 15328 (2017).
949 30 Achim, A. M. *et al.* How prevalent are anxiety disorders in schizophrenia? A meta-analysis and
950 critical review on a significant association. *Schizophr Bull.* **37**, 811–821 (2011).
951 31 Swerdlow, N. R., Braff, D. L., Taaid, N. & Geyer, M. A. Assessing the validity of an animal model
952 of deficient sensorimotor gating in schizophrenic patients. *Arch Gen Psychiatry* **51**, 139–154
953 (1994).
954 32 Light, G. A. & Braff, D. L. Human and animal studies of schizophrenia-related gating deficits.
955 *Curr Psychiatry Rep.* **1**, 31–40 (1999).
956 33 van den Buuse, M. Modeling the positive symptoms of schizophrenia in genetically modified
957 mice: pharmacology and methodology aspects. *Schizophr Bull.* **36**, 246–270 (2010).
958 34 Rahimian, R., Wakid, M., O'Leary, L. A. & Mechawar, N. The emerging tale of microglia in
959 psychiatric disorders. *Neurosci Biobehav Rev.* **131**, 1–29 (2021).
960 35 Borst, K., Dumas, A. A. & Prinz, M. Microglia: Immune and non-immune functions. *Immunity.*
961 **54**, 2194–2208 (2021).
962 36 Sellgren, C. M. *et al.* Increased synapse elimination by microglia in schizophrenia patient-
963 derived models of synaptic pruning. *Nat Neurosci.* **22**, 374 (2019).
964 37 Müller, N., Weidinger, E., Leitner, B. & Schwarz, M. J. The role of inflammation in
965 schizophrenia. *Front Neurosci.* **21**, 372 (2015).
966 38 van Mierlo, H. C., Schot, A., Boks, M. P. M. & de Witte, L. D. The association between
967 schizophrenia and the immune system: Review of the evidence from unbiased 'omic-studies'.
968 *Schizophr Res.* **217** (2020).
969 39 Sharma, R. P., Rosen, C., Melbourne, J. K., Feiner, B. & Chase, K. A. 2016.
970 *Neuroimmunomodulation* **23**, 224–229
971 40 Muendlein, H. I. *et al.* ZBP1 promotes LPS-induced cell death and IL-1 β release via RHIM-
972 mediated interactions with RIPK1. *Nat Commun.* **12**, 86 (2021).
973 41 Shao, R. G. *et al.* Necrostatin-1 attenuates Caspase-1-dependent pyroptosis induced by the
974 RIPK1/ZBP1 pathway in ventilator-induced lung injury. *Cytokine* **157**, 155950 (2022).
975 42 de Reuver, R. *et al.* ADAR1 prevents autoinflammation by suppressing spontaneous ZBP1
976 activation. *Nature* **607**, 784–789 (2022).
977 43 Buckley, P. F. Neuroinflammation and Schizophrenia. *Curr Psychiatry Rep* **21**, 72 (2019).
978 44 Rodrigues-Neves, A. C., Ambrósio, A. F. & Gomes, C. A. Microglia sequelae: brain signature of
979 innate immunity in schizophrenia. *Transl Psychiatry.* **12**, 493 (2022).
980 45 Barbato, C. *et al.* Cognitive Decline and Modulation of Alzheimer's Disease-Related Genes
981 After Inhibition of MicroRNA-101 in Mouse Hippocampal Neurons. *Molecular Neurobiology*
982 **57**, 3183–3194 (2020).

983 46 Mundalil Vasu, M. *et al.* Serum microRNA profiles in children with autism. *Molecular autism*
984 **5**, <https://doi.org/10.1186/2040-2392-1185-1140> (2014).

985 47 Zadehbagheri, F., Hosseini, E., Bagheri-Hosseinabadi, Z., Reabdarkolae, H. M. & Sadeghi, I.
986 Profiling of miRNAs in serum of children with attention-deficit hyperactivity disorder shows
987 significant alterations. *Journal of psychiatric research* **109**, 185-192 (2019).

988 48 Zhu, H. & Leung, S. W. MicroRNA biomarkers of type 2 diabetes: evidence synthesis from
989 meta-analyses and pathway modelling. *Diabetologia* **66**, 288-299 (2023).

990 49 Zahari Sham, S. Y. *et al.* Circulating miRNAs in Type 2 Diabetic Patients with and without
991 Albuminuria in Malaysia. *Kidney & blood pressure research* **47**, 81-93 (2022).

992 50 Moshiri, F. *et al.* Circulating miR-106b-3p, miR-101-3p and miR-1246 as diagnostic biomarkers
993 of hepatocellular carcinoma. *Oncotarget* **9**, 15350-15364 (2018).

994 51 Zhang, Y., Zhang, P. & Deng, C. miR-378a-5p regulates CAMKK2/AMPK pathway to contribute
995 to cerebral ischemia/reperfusion injury-induced neuronal apoptosis. *Folia histochemica et*
996 *cytobiologica* **59**, 57-65 (2021).

997 52 Biselli, J. M. *et al.* Differential microRNA expression profile in blood of children with Down
998 syndrome suggests a role in immunological dysfunction. *Human cell* **35**, 639-648 (2022).

999 53 Dong, Z. *et al.* Profiling of Serum Exosome MiRNA Reveals the Potential of a MiRNA Panel as
1000 Diagnostic Biomarker for Alzheimer's Disease. *Molecular Neurobiology* **58**, 3084-3094 (2021).

1001 54 Chen, S. D. *et al.* A preliminary analysis of microRNA-21 expression alteration after
1002 antipsychotic treatment in patients with schizophrenia. *Psychiatry research* **244**, 324-332
1003 (2016).

1004 55 Maffioletti, E. *et al.* Peripheral whole blood microRNA alterations in major depression and
1005 bipolar disorder. *Journal of affective disorders* **200**, 250-258 (2016).

1006 56 Vykoukal, J. *et al.* Contributions of Circulating microRNAs for Early Detection of Lung Cancer.
1007 *Cancers* **14**, 4221 (2022).

1008 57 Qin, Z., Han, X., Ran, J., Guo, S. & Lv, L. Exercise-Mediated Alteration of miR-192-5p Is
1009 Associated with Cognitive Improvement in Alzheimer's Disease. *Neuroimmunomodulation* **29**,
1010 36-43 (2022).

1011 58 Yoshino, Y., Roy, B. & Dwivedi, Y. Differential and unique patterns of synaptic miRNA
1012 expression in dorsolateral prefrontal cortex of depressed subjects.
1013 *Neuropsychopharmacology* **46**, 900-910 (2021).

1014 59 Tang, C. Z., Yang, J. T., Liu, Q. H., Wang, Y. R. & Wang, W. S. Up-regulated miR-192-5p
1015 expression rescues cognitive impairment and restores neural function in mice with depression
1016 via the Fbln2-mediated TGF- β 1 signaling pathway. *FASEB J* **33**, 606-618 (2019).

1017 60 Van der Auwera, S. *et al.* Association of childhood traumatization and neuropsychiatric
1018 outcomes with altered plasma micro RNA-levels. *Neuropsychopharmacology* **44**, 2030-2037
1019 (2019).

1020 61 Huang, Z. X., Chen, Y., Guo, H. R. & Chen, G. F. Systematic Review and Bioinformatic Analysis
1021 of microRNA Expression in Autism Spectrum Disorder Identifies Pathways Associated With
1022 Cancer, Metabolism, Cell Signaling, and Cell Adhesion. *Frontiers in Psychiatry* **12**, 630876
1023 (2021).

1024 62 Banach, E., Szczepankiewicz, A., Kaczmarek, L., Jaworski, T. & Urban-Ciećko, J. Dysregulation
1025 of miRNAs Levels in Glycogen Synthase Kinase-3 β Overexpressing Mice and the Role of miR-
1026 221-5p in Synaptic Function. *Neuroscience* **490**, 287-295 (2022).

1027 63 van Heukelum, S. *et al.* Where is Cingulate Cortex? A Cross-Species View. *Trends Neurosci.* **43**,
1028 285-299 (2020).

1029 64 Feifel, D. & Shilling, P. D. Promise and pitfalls of animal models of schizophrenia. *Psychiatry*
1030 *Rep* **12**, 327-334 (2010).

1031 65 Bayer, T. A., Buslei, R., Havas, L. & Falkai, P. Evidence for activation of microglia in patients
1032 with psychiatric illnesses. *Neurosci Lett.* **271**, 126-128 (1999).

1033 66 Benros, M. E. *et al.* Autoimmune diseases and severe infections as risk factors for
1034 schizophrenia: a
1035 30-year population-based register study. *Am J Psychiatry* **168** (2011).
1036 67 van Berckel, B. N. *et al.* Microglia activation in recent-onset schizophrenia: a quantitative (R)-
1037 [11 C]PK11195 positron emission tomography study. *Biol Psychiatry*. **64**, 820-822 (2008).
1038 68 Ottoy, J. *et al.* (18)F-PBR111 PET imaging in healthy controls and schizophrenia: test-retest
1039 reproducibility and quantification of neuroinflammation. *J Nucl Med*. 2018;59:1267–74. *J Nucl*
1040 *Med*. **59**, 1267-1274 (2018).
1041 69 Juckel, G. *et al.* Microglial activation in a neuroinflammatory animal model of schizophrenia—a
1042 pilot study. *Schizophr Res*. **131**, 96-100 (2011).
1043 70 Shelton, H. W. *et al.* The effects of a novel inhibitor of tumor necrosis factor (TNF) alpha on
1044 prepulse inhibition and microglial activation in two distinct rodent models of schizophrenia.
1045 *Behav Brain Res* **406**, 113229 (2021).
1046 71 Wang, L. *et al.* Targeted delivery of miR-99b reprograms tumor-associated macrophage
1047 phenotype leading to tumor regression. *J Immunother Cancer* **8**, :e000517 (2020).
1048 72 Singh, Y. *et al.* Mycobacterium tuberculosis controls microRNA-99b (miR-99b) expression in
1049 infected murine dendritic cells to modulate host immunity. *J Biol Chem*. **288**, 5056-5061
1050 (2013).
1051 73 Momtazmanesh, S., Zare-Shahabadi, A. & Rezaei, N. Cytokine Alterations in Schizophrenia: An
1052 Updated Review. *Front Psychiatry*. **10**, doi: 10.3389/ (2019).
1053 74 Vilalta, A. & Brown, G. C. Neurophagy, the phagocytosis of live neurons and synapses by glia,
1054 contributes to brain development and disease. *FEBS J*. **285**, 3566-3575 (2018).
1055 75 Inta, D., Lang, U. E., Borgwardt, S., Meyer-Lindenberg, A. & Gass, P. Microglia Activation and
1056 Schizophrenia: Lessons From the Effects of Minocycline on Postnatal Neurogenesis, Neuronal
1057 Survival and Synaptic Pruning. *Schizophr Bull*. **43**, 493-496 (2017).
1058 76 Germann, M., Brederoo, S. G. & Sommer, I. E. C. Abnormal synaptic pruning during
1059 adolescence underlying the development of psychotic disorders. *Curr Opin Psychiatry* **34**, 222-
1060 227 (2021).
1061 77 Takaoka, A. *et al.* DAI (DLM-1/ZBP1) is a cytosolic DNA sensor and an activator of innate
1062 immune response. *Nature* **448**, 501-505 (2007).
1063 78 Kuriakose, T. *et al.* ZBP1/DAI is an innate sensor of influenza virus triggering the NLRP3
1064 inflammasome and programmed cell death pathways. *Sci Immunol*. **1**, aag2045 (2016).
1065 79 Hong, S. *et al.* Complement and microglia mediate early synapse loss in Alzheimer mouse
1066 models. *Science* **352**, 712-716 (2016).
1067 80 Heneka, M. T. *et al.* NLRP3 is activated in Alzheimer's disease and contributes to pathology in
1068 APP/PS1 mice. *Nature* **493**, 674-678 (2013).
1069 81 Ye, X. *et al.* MicroRNAs 99b-5p/100-5p Regulated by Endoplasmic Reticulum Stress are
1070 Involved in Abeta-Induced Pathologies. *Front Aging Neurosci*. **18**, 210 (2015).
1071 82 Hart, A. D., Wyttenbach, A., Perry, V. H. & Teeling, J. L. Age related changes in microglial
1072 phenotype vary between CNS regions: grey versus white matter differences. *Brain Behav*
1073 *Immun*. **26**, 754-765 (2012).
1074 83 Ayata, P. *et al.* Epigenetic regulation of brain region-specific microglia clearance activity. *Nat*
1075 *Neurosci*. **21**, 1049-1060 (2018).
1076 84 Mustapic, M. *et al.* Plasma Extracellular Vesicles Enriched for Neuronal Origin: A Potential
1077 Window into Brain Pathologic Processes. *Front Neurosci*. **11**, doi: 10.3389/fnins.2017.00278.
1078 (2017).
1079 85 Kumar, A. *et al.* Brain cell-derived exosomes in plasma serve as neurodegeneration biomarkers
1080 in male cynomolgus monkeys self-administering oxycodone. *EBioMedicine* **63**, 103192
1081 (2021).
1082 86 Langfelder, P. & Horvath, S. WGCNA: an R package for weighted correlation network analysis.
1083 *BMC Bioinformatics*. **29**, eCollection (2008).

1084 87 Shannon, P. *et al.* Cytoscape: a software environment for integrated models of biomolecular
1085 interaction networks. *Genome Research* **13**, 2498-2504 (2003).
1086 <https://doi.org/10.1101/gr.1239303>
1087 88 Bindea, G. *et al.* ClueGO: a Cytoscape plug-in to decipher functionally grouped gene ontology
1088 and pathway annotation networks. *Bioinformatics* **25**, 1091-1093 (2009).
1089 89 McKenzie, A. T. *et al.* Brain Cell Type Specific Gene Expression and Co-expression Network
1090 Architectures. *Scientific reports* **8**, 8868 (2018).
1091 90 Ortutay, C. & Vihinen, M. Immunome: A reference set of genes and proteins for systems
1092 biology of the human immune system. *Cellular Immunology* **244**, 87-89 (2006).
1093 91 Abbas, A. R. *et al.* Immune response in silico (IRIS): immune-specific genes identified from a
1094 compendium of microarray expression data. *Genes and immunity* **6**, 319-331 (2005).
1095 92 Islam, M. R. *et al.* A microRNA signature that correlates with cognition and is a target against
1096 cognitive decline. *EMBO molecular medicine* **13**, e13659 (2021).
1097 <https://doi.org/10.15252/emmm.202013659>
1098 93 Pantazis, C. B. *et al.* A reference human induced pluripotent stem cell line for large-scale
1099 collaborative studies. *Cell stem cell* **29**, 1685-1702 (2022).
1100 94 Haenseler, W. *et al.* A Highly Efficient Human Pluripotent Stem Cell Microglia Model Displays
1101 a Neuronal-Co-culture-Specific Expression Profile and Inflammatory Response. *Stem cell*
1102 *reports* **8**, 1727-1742 (2017).
1103 95 Goldberg, M. *et al.* Exercise as a model to identify microRNAs linked to human cognition: A
1104 role for microRNA-409 and microRNA-501. *Translational Psychiatry* **11**, 514 (2021).
1105

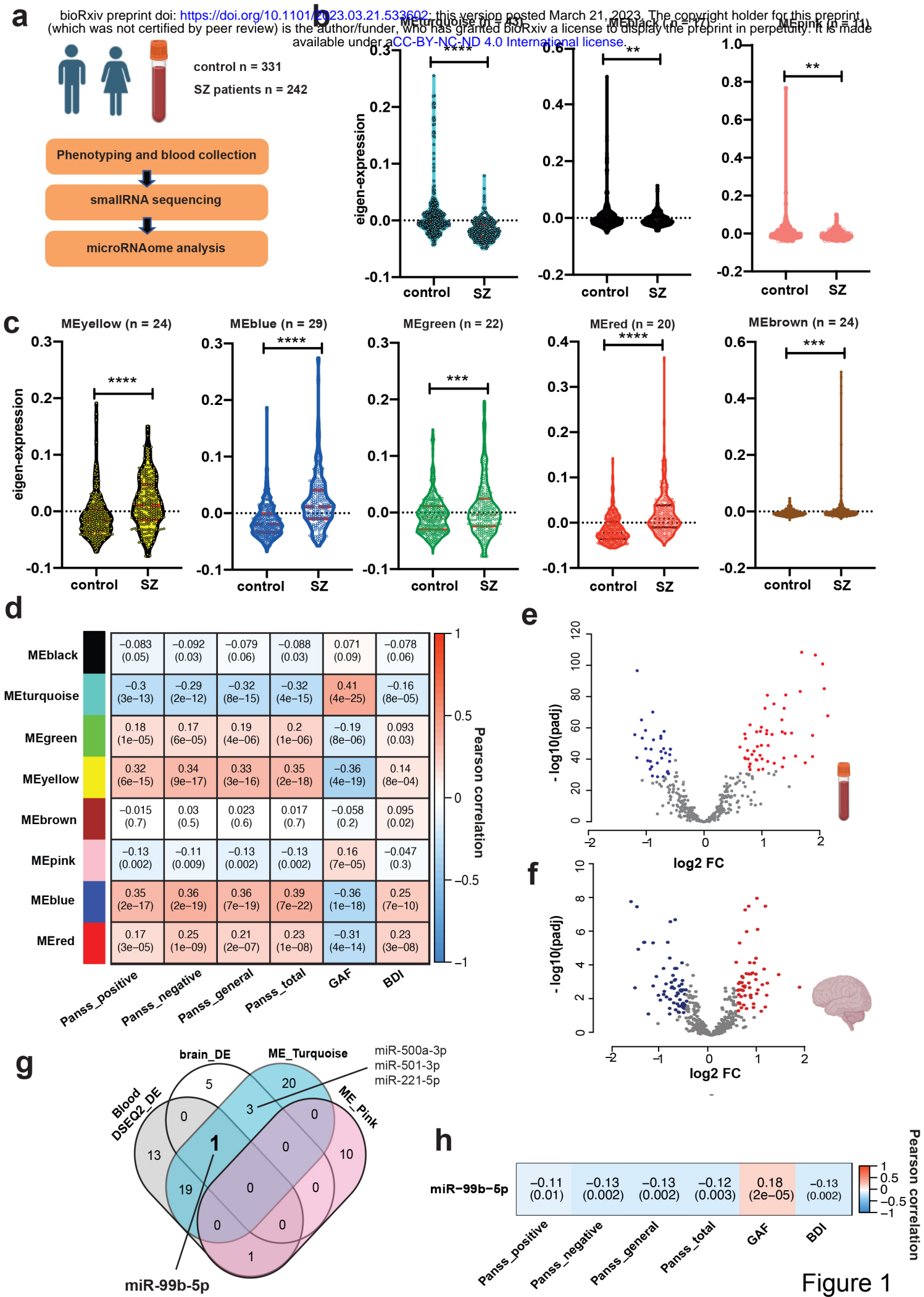


Figure 1

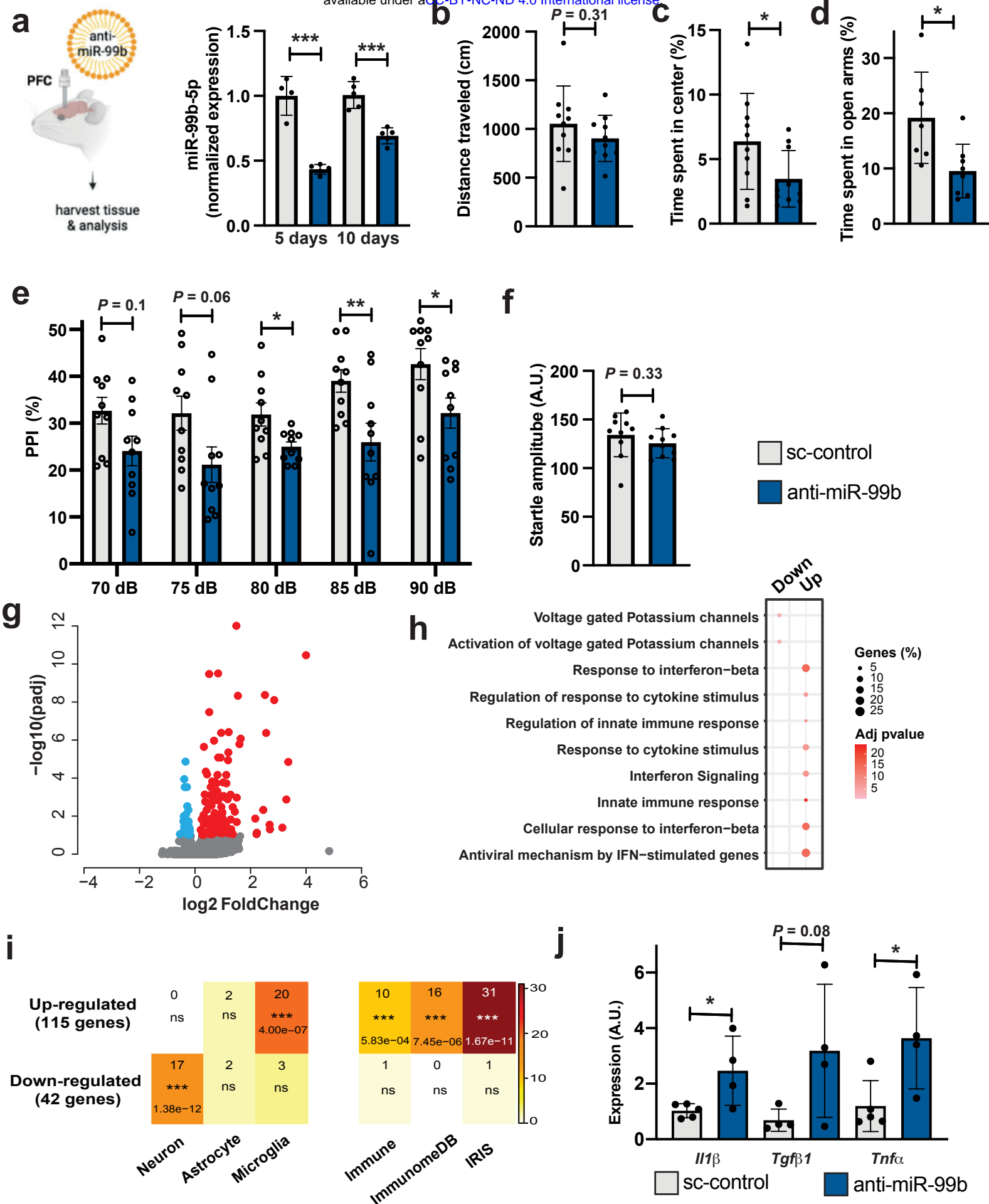


Figure 2

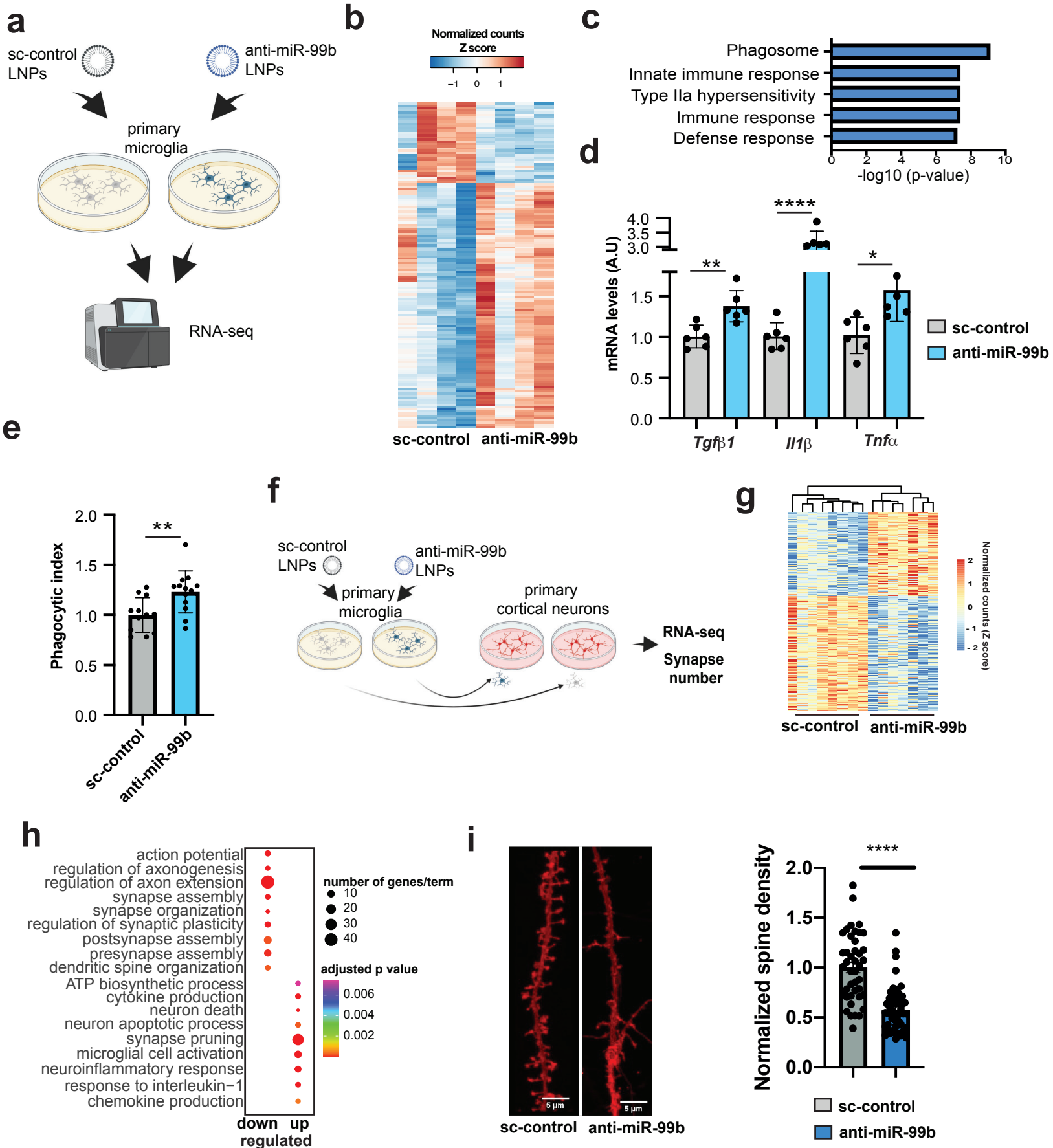


Figure 3

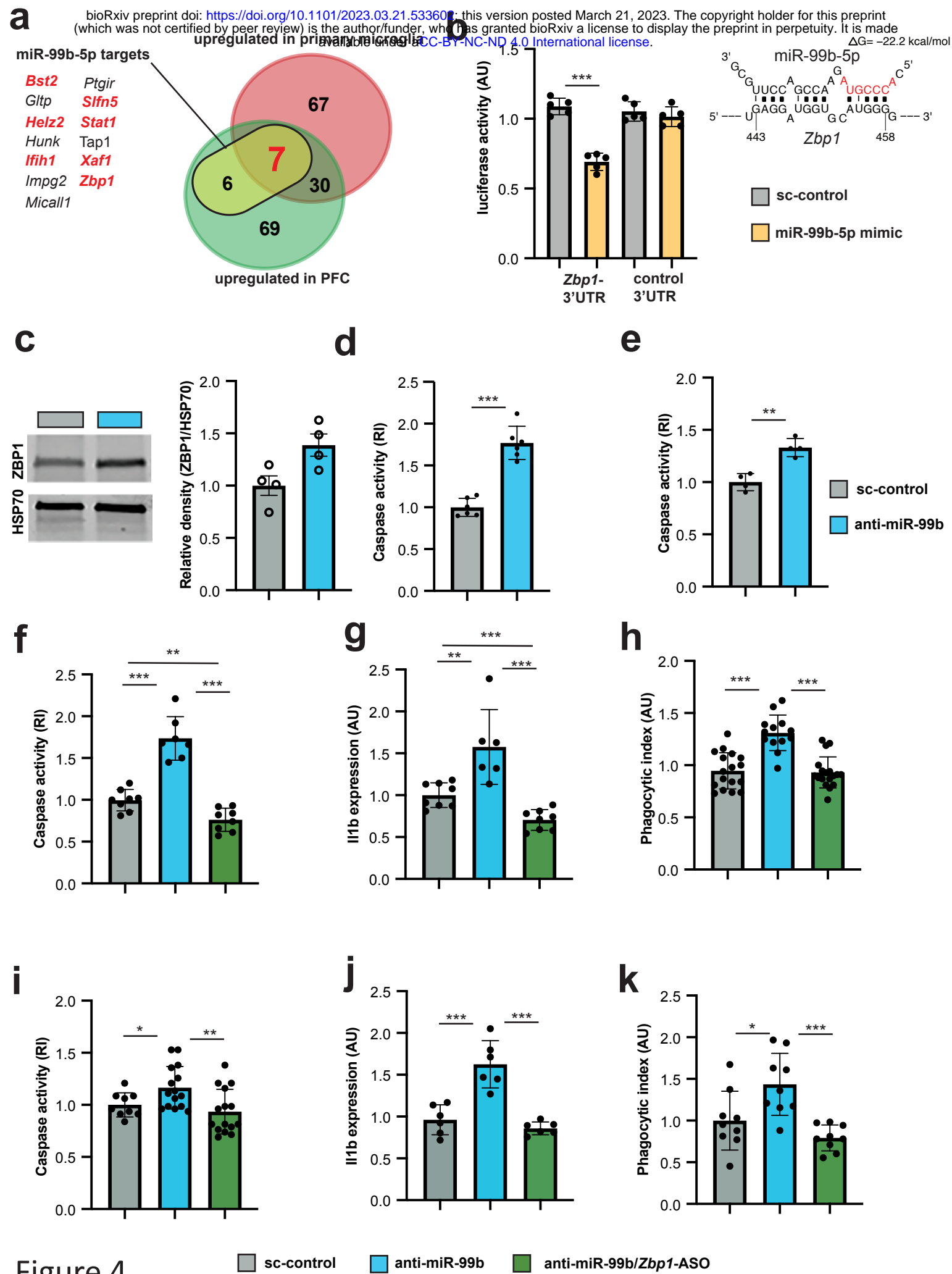


Figure 4